Miner Deposita (2009) 44:559–580
DOI 10.1007/s00126-008-0220-4

ARTICLE

Nonsulfide zinc deposits in the Silesia–Cracow district, Southern Poland

Vito Coppola · Maria Boni · H. Albert Gilg · Bozena Strzelska-Smakowska

Received: 17 April 2008 / Accepted: 29 October 2008 / Published online: 29 November 2008

Abstract The Silesia–Cracow district in Poland has been one of the world's principal sources of zinc from nonsulfide zinc ore (Polish: *galman*). The still remaining nonsulfide ore resources can be estimated at 57 Mt at 5.6% Zn and 1.4% Pb. Nonsulfide mineralization is mainly hosted by Lower Muschelkalk (Triassic) limestone and is associated with different generations of the hydrothermal ore-bearing dolomite (OBD I, II, III). A fundamental ore control is believed to have been exerted by the basement faults, which were repeatedly reactivated during the Alpine tectonic cycle, leading to the formation of *horst*-and-*graben* structures: these dislocations may have caused short periods of emersion and the circulation of meteoric waters during the Cenozoic. Nonsulfide ores show a wide range of morphological characteristics and textures. They occur as earthy masses, crystalline aggregates, and concretions in cavities. Breccia and replacement textures are also very common. The most important mineral phases are: smithsonite, Fe–smithsonite, Zn–dolomite, goethite, and Fe–Mn (hydr)oxides. Minor hemimorphite and hydrozincite have also been detected. Two distinct nonsulfide ore types occur: the predominant *red galman* and the rare *white galman*. In the *white galman*, Fe–smithsonite and Zn–dolomite are particularly abundant. This ore type is commonly considered as a peripheral hydrothermal alteration product related to the same fluids that precipitated both the OBD II–III and the sulfides. In contrast, a supergene origin is commonly assumed for the *red galman*. Evidence of the petrographic and mineralogical difference between *white* and *red galman* is also found in stable isotope data. Smithsonite from *red galman* shows a limited range of $\delta^{13}C_{VPDB}$ values (−10.1 to −11.4‰), and $\delta^{18}O_{VSMOW}$ values (25.3‰ to 28.5‰, mean 26.8±0.3‰). The uniform and low carbon isotope values of *red galman* smithsonite are unusual for supergene carbonate-hosted deposits and indicate the predominance of a single organic carbon source. Smithsonite from *white galman* has a more variable, slightly more positive carbon isotope (−2.9‰ to −7.4‰), but broadly similar oxygen isotope composition (26.8‰ to 28.9‰). The relationship of the *white galman* ore with the hydrothermal system responsible for OBD II and sulfide generation is still uncertain. The most important paleoweathering events took place in both Lower and Upper Silesia during Late Cretaceous up to Paleogene and early Neogene time. During this period, several short-lasting emersions and intense weathering episodes facilitated the formation of sinkholes in the Triassic carbonate rocks and the oxidation of sulfide

Editorial handling: Bernd Lehmann

V. Coppola · M. Boni (✉)
Dipartimento di Scienze della Terra,
Università di Napoli "Federico II",
Via Mezzocannone 8,
80134 Napoli, Italy
e-mail: boni@unina.it

V. Coppola
e-mail: coppola_vito@hotmail.com

H. A. Gilg
Lehrstuhl für Ingenieurgeologie,
Technische Universität München,
Arcisstr. 21,
80333 Munich, Germany
e-mail: agilg@tum.de

B. Strzelska-Smakowska
Academy of Mining and Metallurgy,
Al. Mickiewicza 30,
30-059 Cracow, Poland
e-mail: Wodnik@geol.agh.edu.pl

M. Boni
Geologisch-Paläontologisches Institut, Universität Heidelberg,
Heidelberg, Germany

orebodies through percolating meteoric waters. These phenomena may have lasted until the Middle Miocene.

Keywords Silesia–Cracow Poland · Nonsulfide zinc · Paleoweathering · Smithsonite · Stable isotopes

Introduction

The Silesia–Cracow ore district represents one of the major European zinc–lead (silver) mining districts (Fig. 1). Mining activity dates back to the beginning of the Polish Kingdom, at least from the eleventh century. At the beginning of the nineteenth century, this district was the source of 40% of the zinc produced worldwide. An important increase in mining activity in Poland has been recorded after World War II, when a new evaluation of the existing Zn–Pb resources was conducted at the mines of Orzel Bialy, Marchlewski, Warynski, Nowy Dwor, Matylda, and adjacent areas. Additional mines were also opened: Boleslaw (1953), Trzebionka (1962), Olkusz (1968) and Pomorzany (1974). The annual production of Zn–Pb ores in the district increased from about 500,000 tonnes/year during the period between the two world wars, up to about 5 Mt in 1980 when 188,000 tonnes of zinc and 47,500 tonnes of lead in concentrates were produced from the Silesia–Cracow mines (Gruszczyk and Wielgomas 1987). The zinc production included both sulfide concentrate and roasted nonsulfides.

Currently, the mining activity in the district is restricted to a few sulfide deposits, with estimated sulfide ore reserves in 2006 of 168 Mt at 3.87% Zn and 1.78% Pb (Polish Minerals Yearbook 2007). Nonsulfide ores are currently not exploited, contrary to the first part of the twentieth century, when a part of this district—Upper Silesia—belonged to Germany. However, these nonsulfide ores are far from being exhausted. They have been estimated to contain 57 Mt at 5.6% Zn and 1.4% Pb (Kucha 2005).

Research on nonsulfide Zn ores (called "*galman*," which is a modification of the German name "*Galmei*") has been carried out intensively in the past decades (Zabinski 1960; Szuwarzynski 1978; Radwanek-Bak 1983; Osman 1989). However, many mineralogical and geological characteristics of the "*galman*" ores in the Silesia–Cracow district are still not fully documented, and their ages are not precisely known. Research indicates that most of these ores (*"red galman"*) represent the supergene oxidation products of primary sulfides. However, it cannot be ruled out that some nonsulfide concentrations (*"white galman"*) may be of different origin. Based on geological constraints, their emplacement age ranges between that of primary sulfide mineralization (Jurassic? Cretaceous? Tertiary?) and the deposition of a discontinuous sedimentary cover of Miocene age (Smakowski and Strzelska-Smakowska 2005).

The mineralogical assemblage of the ores includes smithsonite as the most abundant mineral, but also Fe–smithsonite, hemimorphite, hydrozincite, Zn–dolomite, cerussite, goethite, anglesite, hydrous Zn- and Pb-sulfates, phosphates, and remnants of primary sulfides (Zabinski 1960; Bak and Nieć 1978; Bak and Zabinski 1981). An epigenetic dolomite (OBD), which has pervasively replaced the Triassic limestones, represents the prevailing host rock

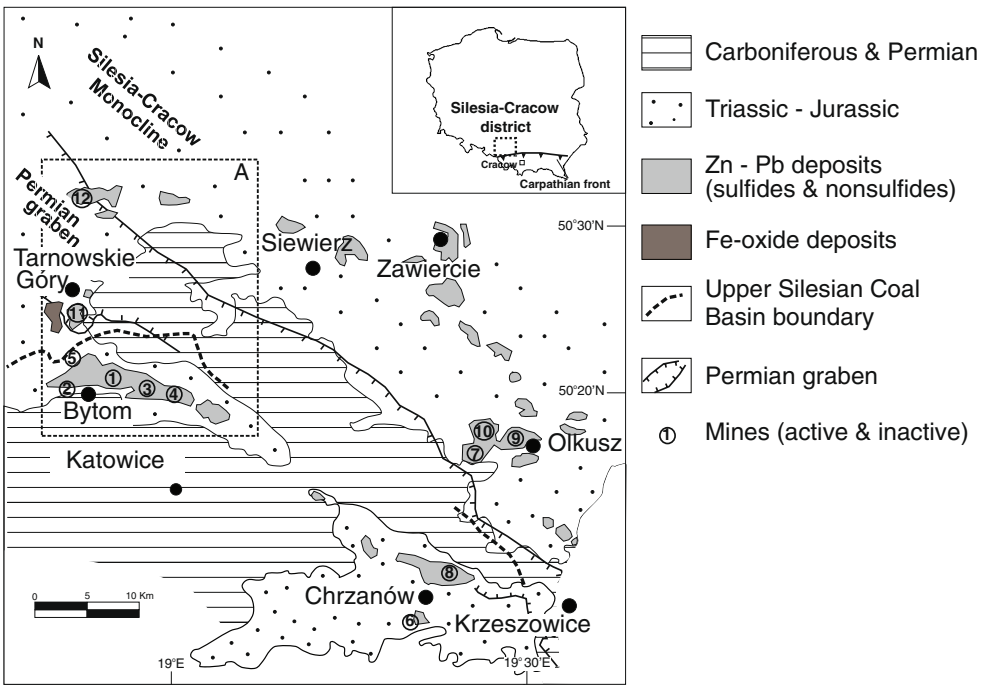

Fig. 1 Schematic geological map of the Silesia–Cracow mining district. Both exploited and undeveloped deposits are shown in the map. *1* Warynski, *2* Marchlewski, *3* Orzel Bialy, *4* Dabrowka, *5* Nowy Dwor, *6* Matylda, *7* Boleslaw, *8* Trzebionka, *9* Olkusz, *10* Pomorzany, *11* Fryderyk, *12* Bibiela-Kalety. *Frame A* locates the area represented in Fig. 4

for both sulfide and nonsulfide ores in more than 90% of the mineralized areas.

We carried out a detailed mineralogical–petrographic investigation of the nonsulfide ores, paired with stable isotope (O, C) data, to constrain the nature of the fluids involved in the mineralizing process and draw a distinction between "*white*" and "*red*" galman. We also present here a short review of the possible genetic mechanisms and ages of the Polish nonsulfides, interpreted within the framework of the paleoweathering history of the European continent.

Geological setting

The Silesia–Cracow district in southern Poland is located north of the Carpathian overthrust front (Fig. 1), overlapping in part the Upper Silesia Coal Basin. The Zn–Pb deposits occur in the Mesozoic sedimentary cover of the Paleozoic basement of the Central European Platform and are almost completely hosted by carbonate successions of Middle Triassic age (Muschelkalk). The OBD, which is the prevailing host rock of the Zn–Pb ore deposits, though epigenetic in origin, has been formally included in the Muschelkalk succession (Assmann 1944).

The Muschelkalk carbonate sediments have been subdivided into several members (or "beds" in the common literature) named: Gogolin, Gorazdze, Karchowice, Diplopora, Tarnowice, and Boruszowice (Assmann 1944; Kotlicki and Kubicz 1974; Wyczolkowski 1974) (Fig. 2), consisting originally of limestone and/or early diagenetic dolomite (Bogacz et al. 1975; Gorecka 1993). The Muschelkalk sequence is covered by claystone belonging to the Keuper lithologies (Upper Triassic) (Sass-Gustkiewicz et al. 1982). At the boundary between Muschelkalk and Keuper, an erosional paleo-morphology occurs. This morphology affects the Muschelkalk carbonates and locally reaches the lower members of Gogolin beds (Gruszczyk and Paulo 1976; Wilk 1989 and references therein) removing up to 80 m of the carbonate sequence. The Alpine orogeny, which is responsible for the current structure of the Carpathian chain, started in Late Cretaceous and lasted until Late Miocene. Three important Alpine tectonic "phases" can be distinguished in the Silesia–Cracow district (Gorecka 1993): two Early Alpine (Early Cimmerian, and "Laramide") compressional movements and a Late Alpine (Early Tertiary–Miocene) compression. During the Tertiary, the whole area was characterized by block faulting, which resulted in a fault network with N–S and E–W striking directions and vertical offsets around 50–70 m (Dzulynski 1953; Felisiak 1992; Gorecka 1993; Leach et al. 1996). The fault orientation generally follows old tectonic lines of the basement (Gorecka 1993), which were repeatedly reactivated. The dislocations caused short periods of emersion, with related erosion and weathering, alternating with local ingressions. According to Szuwarzynski (1978), the Early Tertiary climatic conditions were favorable to erosion and dissolution, thus resulting in the removal of Mesozoic and Paleogene successions and the creation of erosion surfaces paired with a deep karst morphology. A very intense weathering phase accompanied by karst dissolution and numerous sinkholes has been recorded in the Chrzanów area before the Middle Miocene (Tortonian) transgression (Panek and Szuwarzynski 1975, 1976; Sobczynski et al. 1978; Sass-Gustkiewicz et al. 1982; Szuwarzynski 1993). The sinkholes were filled by an argillaceous residuum derived from the dissolution of Triassic, Jurassic, and Paleogene carbonate rocks, chert clasts, fine-grained quartz sands and travertines (Panek and Szuwarzynski 1975), as well as by detrital fragments of sulfide and nonsulfide ores (Szuwarzynski 1978) (Fig. 3). The filled sinkholes are capped, especially in the Chrzanów Trough (Radwanski 1968; Alexandrowicz 1969; Szuwarzynski 1978), but also in the Bytom and Tarnowskie Góry region (Gürich 1897), by Tortonian marine claystone (Fig. 3). A discontinuous cover of Quaternary sediments on the nonsulfide ores occurs in the whole mining district.

Ore-bearing dolomite and Zn–Pb sulfide ores

Two generations of OBD have been described in the mining district by Szuwarzynski (1978), Leach et al. (1996), and Heijlen et al. (2003). The first generation (OBD I) consists of a burial dolomite, poor in Fe and Zn, which replaces the Lower Muschelkalk limestone (Gorazdze, Terebratula, and Karchowice beds) and/or the early diagenetic dolomite (which is absolutely barren of metals). OBD I occurs in the form of tabular bodies, commonly located between the Upper Gogolin bed (below) and the Diplopora Dolomite (above; Fig. 2). The dolomitization process causing the formation of OBD I is considered to pre-date the emplacement of sulfide ores, as well as the deposition of the Jurassic sediments (Sass-Gustkiewicz and Dzulyński 1998). The second dolomite generation (OBD II; Bak 1993) forms halos usually a few hundred meters wide around the sulfide ore bodies (Fig. 2). These two dolomite generations also have a different geochemical signature: iron-poor (OBD I) and iron-rich (OBD II) Heijlen et al. 2003. Zinc-rich dolomite (comparable to the iron-rich OBD II) has been described by Zabinski (1980, 1986) from the Chrzanów area, and by Zabinski (1959) and Rosenberg and Champness (1989) from the Warynski mine (Bytom area). In this paper, we will use the term OBD I when referring to the earlier dolomite generation, which pre-dates the main mineralizing event, and OBD II, when referring to the metal-bearing dolomites associated with sulfide ores (albeit

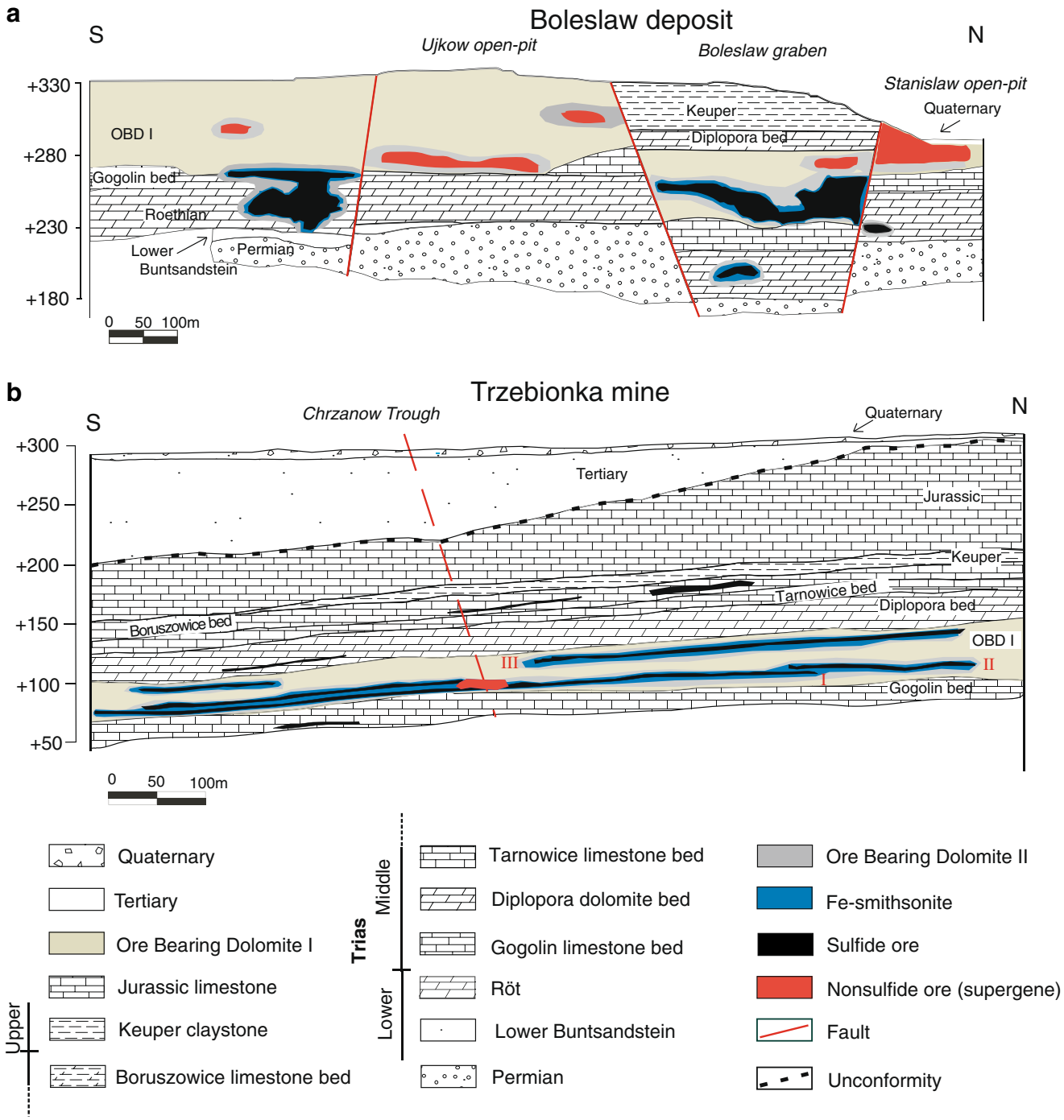

Fig. 2 **a** N–S schematic cross-section of the Boleslaw deposits; **b** N–S schematic cross-section of the Trzebionka mine: *I* mineralized horizon I, *II* mineralized horizon II, *III* mineralized horizon III (see text)

with some difference with respect to the definition of Bak 1993).

Cold cathodoluminescence observation highlighted further differences between dolomite generations I and II. Specifically, OBD I has a dark red or no luminescence, while OBD II shows a red to orange-zoned luminescence. An even younger dolomite generation occurs as well, here named OBD III (Fig. 7e). This late dolomite shows clear signs of subsequent internal dissolution—generally, its crystals are hollow, leaving in place only the external rhombohedral frame (Fig. 6g). Local infilling of these frames primarily consists of smectites and quartz. The empty crystal frames can also be filled by late calcite and by Fe–Mn(hydr)oxides along the cleav-

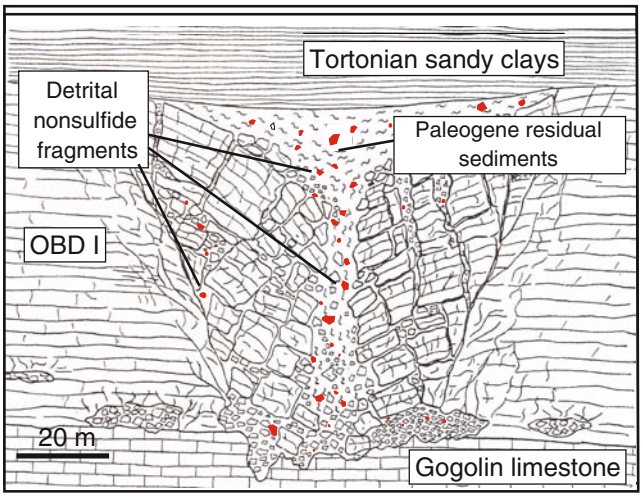

Fig. 3 Sinkhole in Gogolin limestone and OBD I filled with Paleogene sediments, clasts of galena, and nonsulfide fragments in the Chrzanów area (modified from Panek and Szuwarzynski 1975)

ages, or by an orange-luminescing Zn- and Fe-bearing carbonate phase.

Zn–Pb sulfide ores exploitation in the Silesia–Cracow district is still active in two mines: Olkusz–Pomorzany and Trzebionka (Figs. 1 and 2). Even though most sulfides occur in the Muschelkalk–OBD lithologies, smaller Zn–Pb orebodies are locally present in Devonian and Röt dolomites.

Several authors (Sass-Gustkiewicz 1996; Sass-Gustkiewicz et al. 1982; Sass-Gustkiewicz and Dzulyński 1998; Leach and Viets 1992; Gorecka et al. 1996; Leach et al. 1996) have described two mineralization types: (a) stratabound bodies replacing the host carbonates and (b) in-filling of open spaces in fractures and breccias, with banded colloform textures (Fig. 5a). The sulfide bodies are surrounded by a large halo of OBD II and locally by Fe–smithsonite ± (barite; Bak 1993). The mineralogy of the sulfide ores consists of several generations of sphalerite, galena, marcasite, and pyrite locally associated with sulfoarsenides. The last sphalerite and marcasite generations occur in open spaces in the form of stalactites and dripstones containing organic matter. Brunckite has also been found as unconsolidated sediment, consisting of <15 μm particles in fractures and faults at the Trzebionka mine. Sulfide minerals from the ore district have the largest range of sulfur isotope compositions among any Mississippi Valley-type ore district in the world, with the late generations bearing distinctly negative values (−2% to −15% $\delta^{34}S$; brunckite has values as low as −37%; Leach et al. 1996).

An epigenetic hydrothermal MVT-style origin of the Polish sulfide deposits is by now accepted by almost all authors, but their emplacement age is still highly controversial. Three age groups have been proposed for the timing of the main Zn–Pb mineralizing event. Sass-Gustkiewicz and Dzulyński (1998) and Sass-Gustkiewicz et al. (1982), on the basis of geological constraints, consider the age of the main mineralizing event to span the Late Triassic to Middle Jurassic interval. Leach et al. (1996, 2001), propose that all sulfide deposits of the Silesia–Cracow district (from the Devonian—through the Mesozoic to the Tertiary-hosted ores) were formed in a single mineralizing event in Early Tertiary time, which lasted only about 50 Ma. This is supported by isotopic, geochemical, and especially by paleomagnetic studies (Church et al. 1996; Leach et al. 1996; Symons et al. 1995; Viets et al. 1996; Różkowski et al. 1979). Heijlen et al. (2003) assigned an age of 135± 4 Ma to the main mineralizing phase on the basis of direct Rb–Sr dating of sphalerite. The latter authors consider both hydrothermal dolomitization (OBD II) and sulfide deposition to have been caused by Early Cretaceous extension processes, connected to the opening of the Northern Atlantic Ocean.

Nonsulfide zinc ores

Nonsulfide Zn ores occur in several clusters (Fig. 1): in the Chrzanów–Trzebinia–Krzeszowice area, in the Olkusz region (Boleslaw, Olkusz, Pomorzany mines), in the Tarnowskie Gory (Fryderyk mine and "limonitic" nests exploited in the mid-nineteenth century), and in the Bytom trough (Nowy Dwor, Orzel Bialy, Warynski, Marchlewski, Dabrowka mines). The nonsulfides form layers, nests, and lenses throughout the whole OBD I, from the basal contact with the Gogolin Limestone up to the upper contact with the overlying Diplopora Dolomite (Fig. 2).

In the western part of the district (Tarnowskie Gory and Bytom area; Figs. 1 and 4), different types of ores occur: "*limonite*" or "*Brauneisen*" (Gürich 1897) (= goethite-rich oxidized iron ore), galena, sulfides, and *galman*. Silver-bearing galena and "*limonite*" prevail in the Tarnowskie Gory district, while the *galman* and sphalerite ores are particularly abundant in the Bytom area (Fig. 4). The "*galmans*" consist of mixtures of Zn- and Pb-carbonates like smithsonite, ferrous smithsonite (formerly called *monheimite*, Zabinski 1960; Bak and Nieć 1978), Zn–dolomite, cerussite, Pb-rich aragonite (so-called *tarnowitzite*, Breithaupt 1841; Palache et al. 1951; Zabinski 1960), but also goethite, hemimorphite, and relicts of primary sulfides, mainly galena. A subdivision has been made (Zabinski 1960) between so-called *white galman* (not very common; Kucha 2005), and highly ferruginous *red galman*, containing goethite and other Fe(hydr)oxides. In *white galman*, Fe–smithsonite is particularly abundant, as well as Zn–dolomite. *White galman* has been recorded mainly in the Matylda mine (Fig. 1), but also from other deposits of the Silesia–Cracow district (i.e., the Bytom trough; Gürich 1897; Zabinski 1958, 1960; Panek and Szuwarzynski 1974; Kucha and Czajka 1984; Kucha 2005; Fig. 4), whilst *red*

galman occurs in the entire district. A supergene origin is commonly accepted for *red galman*, whereas a hydrothermal origin, possibly linked to a late phase of the main sulfide mineralization, has been proposed for *white galman* (Kucha 2005).

In the Olkusz deposit, several sulfide remnants are scattered in the oxidized groundmass (Radwanek-Bak 1983; Gruszczyk and Wielgomas 1987). In this deposit, as in Boleslaw, the main ores are located in a *horst*-and-*graben* structure bounded by normal faults (Fig. 2), a setting described by several authors (Radwanek-Bak 1982; Smakowski and Strzelska-Smakowska 2005). In the uplifted blocks (*horsts*), only nonsulfide deposits occur. In the *graben* areas, the nonsulfides (when present) directly overlie the primary sulfide ores, and occur directly under the Keuper sediments (Fig. 2). The ores at Boleslaw are hosted in the OBD I replacing the Gogolin bed, but smaller bodies were also found in the Röt dolomites (Nieć et al. 1993; Fig. 2).

In the Chrzanów trough, sulfide mining is active only in the Trzebionka mine (Fig. 2), where three horizons of economic importance are hosted by the OBD I replacing different Muschelkalk lithologies. Horizon III (*upper mineralized body*) is hosted in the Karchowice bed, horizon II (*lower mineralized body*) is hosted in the Gorazdze bed, and horizon I is positioned at the boundary between the Gogolin and Gorazdze beds. Also at Chrzanów, banded smithsonite–siderite concentrations have been locally rec-

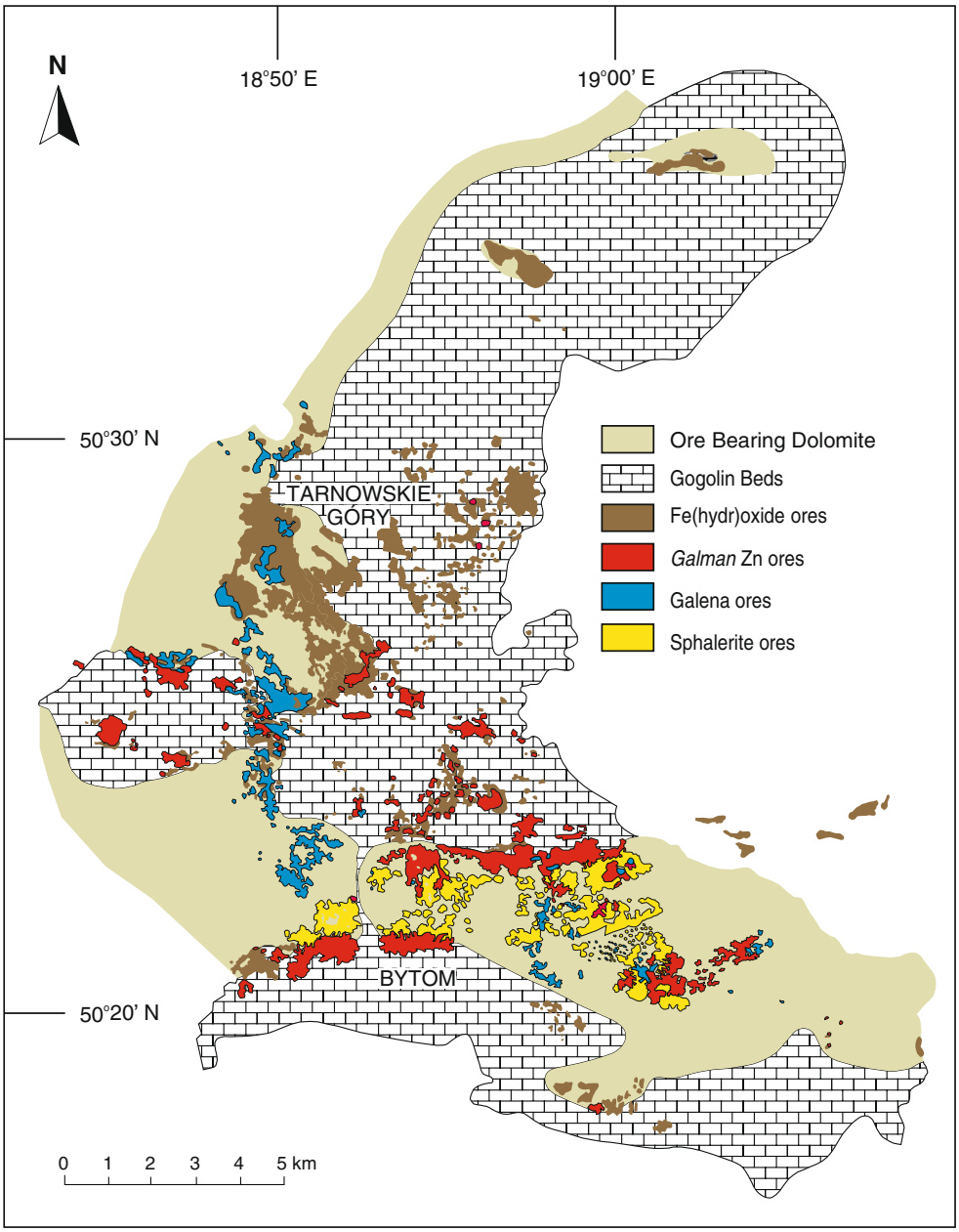

Fig. 4 Geological map of the Bytom–Tarnowskie Gory mining district, with the location of the main ore types (Area A in Fig. 1)

ognized (Kucha and Czajka 1984) at the external front of the sulfide ores. In the Trzebionka mine, sulfide horizons are hosted in OBD I. These show a halo of Zn–dolomite and Fe–dolomite at the contact with the barren host rock (Kucha 2003), while *red galman* forms a noncontinuous layer located immediately above the sulfide bodies.

In the Matylda mine, the nonsulfide ores consisted of several irregular horizons of *white galman* and *red galman* both occurring in the OBD I (Panek and Szuwarzynski 1974; Kucha 2005). The *white galman* was located mostly at the outer part of the deposit or formed patches amidst the *red galman*. The boundaries between *white* and *red galman* were gradational (Smakowski and Strzelska-Smakowska 2005).

Materials and methods

Since many mines are now closed or inaccessible, and good mineralized outcrops are virtually nonexistent, we were unable to collect samples of nonsulfide ores in situ. We gathered most of our samples either in dumps scattered around the old mine sites or from private or mine collections.

Samples in polished thin sections were examined at the Geologisch–Paläontologisches Institut of the Heidelberg University (Germany), by conventional and cold cathodoluminescence petrography using a CITL 8200 Mk3 Cold Cathodoluminescence instrument (23–25 kV voltage and a beam current of 500–550 μA) coupled with an optical microscope.

X-ray powder diffraction analyses (XRPD) were carried out at the Electron Microscopy and Mineral Analysis (EMMA) Division of the Natural History Museum of London (UK). Before analysis, pure mineral phases were separated by a combination of hand picking under a stereomicroscope and gravimetric separation techniques. After separation, all phases were thoroughly cleaned in a sonic bath for 10 min, to eliminate impurities deposited on crystal surfaces. X-ray powder diffraction data were collected using a Nonius PDS120 Powder Diffraction System with an INEL curved position sensitive detector (PSD). This detector has an output array of 4,096 digital channels representing an arc of 120° 2θ and permits the simultaneous measurement of diffracted X-ray intensities at all angles of 2θ across 120° with a static beam-sample-detector geometry. A copper Kα_1 (1.5418Å) radiation was selected for the primary beam using a germanium [111] single-crystal monochromator, and horizontal and vertical slits were used to restrict the beam to a size of 0.24 by 5.0 mm, respectively. Measurements were made in reflection geometry with the powder sample surface at an angle of ~5° to the incident beam. Data collection times were 10 min for each sample, and the angular range recorded was 3–120° 2θ. NIST silicon powder SRM640 was used as an external 2θ calibration standard, and the 2θ linearization of the detector was performed using a least-squares cubic spline function. The STOE Powder Diffraction system software package was used for evaluation of the X-ray diffraction spectrum obtained, compared with the JCPDS-ICDD international database.

SEM observations, as well as the semiquantitative analyses were carried out using the Oxford Instruments INCA on the JEOL 5900LV scanning electron microscope, equipped with an energy-dispersive X-ray spectrometer at the Natural History Museum (London). The instrument working conditions were: 10 mm objective lens to specimen working distance, 6 cm specimen to X-ray detector working distance, X-ray take-off angle to detector 40°, 20 kV accelerating voltage, 2 nA beam current (stabilized and measured with Faraday cup). X-ray matrix correction was carried out automatically by an Oxford Instruments INCA version of the extended Pouchou and Pichoir (XPP) routine. Silicates, sulfates, sulfides, carbonates, oxides, and pure elements were used as standards. Chemical analyses of smithsonite, hemimorphite, cerussite, calcite, and dolomite were performed using a Cameca SX50 electron microprobe with a gas proportional WDS. Instrumental conditions are 15 kV, 15 nA, and 10 μm spot size.

The data were corrected using the PAP program (Pouchou and Pichoir 1991). Minerals and pure elements were used as standard. Also the WDS analyses were carried out at the Electron Microscopy and Mineral Analysis (EMMA) division in the Mineralogy Department of Natural History Museum, London.

Microthermometric analytical measurements on fluid inclusions were carried out at the Dipartimento di Geofisica e Vulcanologia, Università di Napoli, Italy, using a Linkam THMSG 600 heating/freezing stage. The stage was calibrated using synthetic fluid inclusion (Bodnar and Sterner 1987).

Stable oxygen and carbon isotope ratios of carbonates were determined using an automated online device (Finnigan Gasbench II), operated in a continuous flow mode attached to a Finnigan Deltaplus mass spectrometer at the Bayerische Staatssammlung für Paläontologie, Munich, Germany and a Finningan Delta S mass spectrometer at the Ruhr Universität, Bochum, Germany. The purity of handpicked samples was checked by XRD. All carbonate samples were reacted with anhydrous phosphoric acid at 72°C for 1.5 h. Oxygen isotope analyses were corrected using the following phosphoric acid fractionation factors for calcite (1.00864, Swart et al. 1991), dolomite (1.00986, Rosenbaum and Sheppard 1986), cerussite (1.00919, Gilg et al. 2003), and smithsonite (1.00962, Gilg et al. 2003). The precision of analyses based on repeated measurements of laboratory and international standards is about 0.1‰ (1σ). The isotopic compositions are reported as δ-values in per mil. The O isotope compositions of minerals were

expressed relative to VSMOW, and C isotope compositions were expressed relative to VPDB.

Mineralogy of nonsulfide ores

The Polish nonsulfide samples show many textures and morphologies. They occur as earthy (Fig. 5b) to crystalline-looking rocks, crystal aggregates, and concretions in cavities (Fig. 5c). Breccia and replacement textures are very common.

The most important mineralogical phases are: smithsonite, Zn–dolomite, goethite, and Fe–Mn(hydr)oxides (Table 1). Hydrozincite has been found only in some samples collected in the Boleslaw open pit, and in the Pomorzany mine. Hemimorphite is present in most deposits, with the exception of Matylda. Hemimorphite can directly replace sphalerite and form aggregates of euhedral crystals in cavities (Fig. 5a). Rare (Fe- and Zn-) sulfates occurring as very late phases are also common, and clay minerals (mainly Zn–smectites) occur with the oxidation products.

Smithsonite

Smithsonite has been detected in many specimens sampled throughout the whole mining province. Smithsonite cell parameters vary for *a* from 4.644(7) and 4.670 (7) Å and for *c* between 15.036(2) and 15.120(6) Å. These values agree quite well with the data available in the literature (Effenberger et al. 1981; Chang et al. 1995; Boni et al. 2003; Coppola et al. 2008). However, we did not observe a direct relationship between the morphology of the Zn-carbonates, their chemical composition, and the measured cell parameters. XRD analyses also revealed the presence of Fe–smithsonite in the Matylda mine, as evidenced by the value of 2.775(1) Å for the main peak in sample CV05-65.

Hemimorphite

Hemimorphite, less abundant than smithsonite but identified in many deposits, occurs as tabular crystals elongated along the *b* axis. In the specimens from the

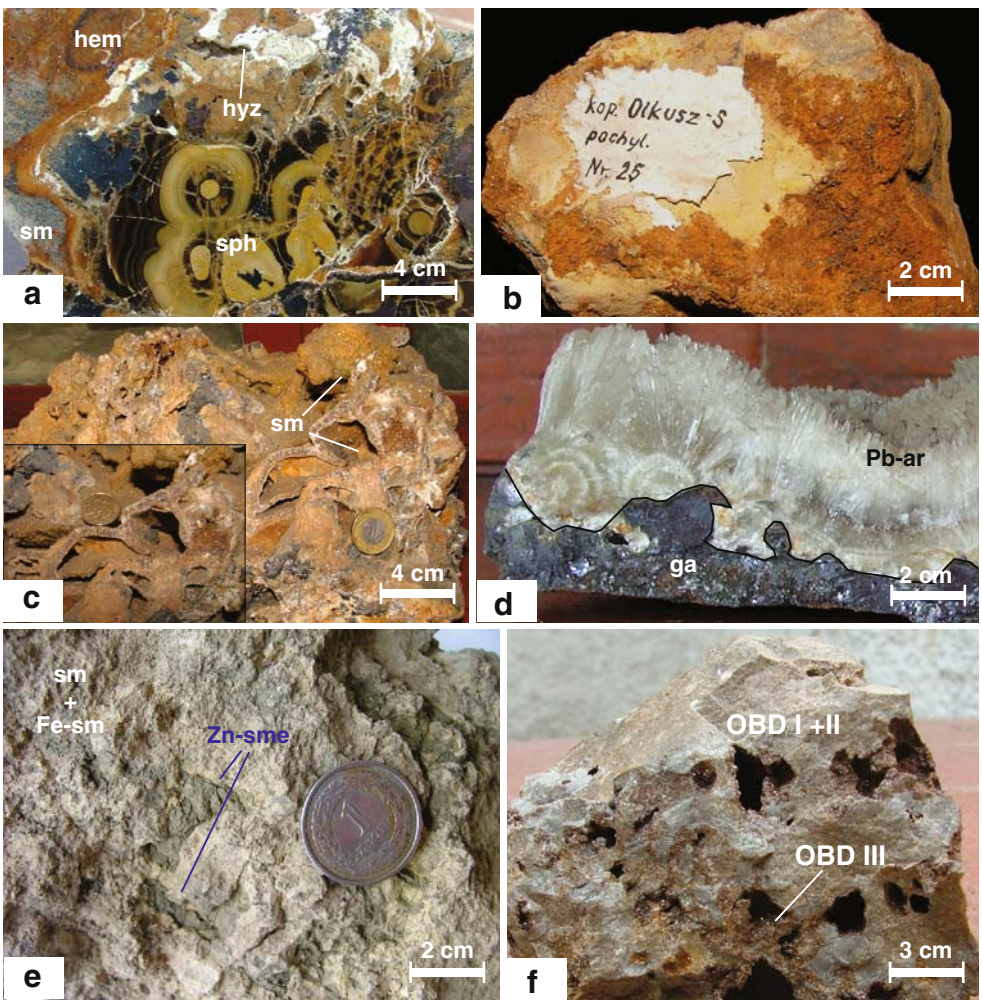

Fig. 5 **a** Banded colloform sphalerite partially replaced by smithsonite (*gray phase*), hemimorphite (*orange phase*) in fractures and hydrozincite (*earthy white*) in cavities. Pomorzany mine −242 m asl (CV05-80); **b** Earthy ore sample with smithsonite and goethite, Olkusz mine (coll. AGH University Cracow); **c** Smithsonite concretion in cavity, Tzrebionka mine (mining company collection); **d** Fibrous Pb–aragonite ("*tarnowitzite*") on galena, Tzrebionka mine (mining company collection); **e** Massive smithsonite and Fe–smithsonite with Zn–smectite (*green*) in a cavity, Matylda mine (CV05-62); **f** Massive OBD (I and II) with late dolomite (OBD III) in cavities, Boleslaw open pit, −280 m asl (CV05–79)

Table 1 XRD analyses of the samples from the Silesia–Cracow district (S Poland)

	Sample	Mineral(s)		Sample	Mineral(s)
Boleslaw	CV05-2	dol, cc, qz, Zn–sme	Pomorzany	CV05-25	dol, qz
	CV05-4	cc, sm, go, qz, do		CV05-53	dol, qz, go, sm
	CV05-6	cc, dol, go, eps		CV05-80	hem, hyz, sm, sph, ce, ga
	CV05-7	do, cc		CV05-83	ga, sph, qz
	CV05-8	cc, qz, go, hyce			
	CV05-9	dol, sm, go	Matylda	CV05-62	Fe–sm, dol, qz, Zn–sme, nk
	CV05-10	cc, sm, do, go, qz, mel, scl		CV05-63	Fe–sm, Zn–sme
	CV05-11	dol, sm, go		CV05-65	Fe–sm, Zn–sme, dol
	CV05-14	dol, sm, hem, go, cc		CV05-73	dol, go
	CV05-15	dol, sm, hem, qz, Zn–sme		CV05-74	dol, go
	CV05-17	dol, sm, do, go, cc, qz		CV05-75	dol, go, qz
	CV05-44	dol, go		CV05-81	sm, dol, qz, Zn–sme
	CV05-45	cc, sm		CV05-85	dol, qz, sm, go, ang
	CV05-49	dol, go, cc, qz, sm		CV05-86	sm, dol, Zn–sme, go, qz
	CV05-50	dol, sm, sch			
	CV05-51	do, cc	Olkusz	CV05-64	dol, sm, sch
	CV05-51b	dol, sm, go		CV05-66	hem, sm
	CV05-58	dol, sm, qz, go, sph, ga		CV05-67	sm, go, qz, hyce
	CV05-59a	sm, dol, go, Zn–sme, qz		CV05-68	ce, ga
	CV05-77	cc, dol, sm, go, hyce			
	CV05-78	cc, do, sm, go	Bibiella	CV05-27	sm, Zn–sme
	CV05-79	dol, cc		CV05-28	dol, sm
				CV05-29	cc, dol, go
Trzebionka	CV05-18	do		CV05-30	sm
	CV05-19	dol, Zn–sme, go, gy		CV05-32	sm, go, dol, gy
	CV05–20	do		CV05-33	sm, dol, hem, Zn–sme
	CV05-52	dol, cc, go, hyce		CV05-34	cc, dol
	CV05-55	cc, Pb-ar		CV05-35	dol, cc, go
	CV05-56	sm		CV05-37	go, he
	CV05-57	hem			
	CV05-60	cc	Szczesé Boze	CV05-46	dol, cc, go, qz
	CV05-82	sm, go, sph, ga, ce, nk			
			Zabinski coll.	CV05-69	cc, go
Bytom	CV05-54	dol, nk		CV05-70	hyz, dol, go, Zn-sme
				CV05-71	sm, hem, ga, sph
Pomorzany	CV05-24	hem, cc, dol, go			

Mineral symbols are in order of abundance
ang anglesite, *Pb–Ar* Pb-rich aragonite, *bass* bassanite, *cc* calcite, *ce* cerussite, *dol* dolomite, *eps* epsomite, *Fe–sm* Fe–smithsonite, *ga* galena, *go* goethite, *gos* goslarite, *gy* gypsum, *he* hematite, *hem* hemimorphite, *hyce* hydrocerussite, *hyz* hydrozincite, *mel* melanterite, *nk* nantokite, *py* pyrite, *qz* quartz, *ros* rosasite, *scl* sclarite, *sch* schafarzikite, *sm* smithsonite, *sph* sphalerite, *Zn–sme* Zn–smectite

Boleslaw open pit, hemimorphite forms concretions growing in cavities on the rhombohedral dolomite crystals and/or on the previously deposited smithsonite. Crystal sizes range from a few micrometers to 400 μm. In the specimens from the Pomorzany mine, hemimorphite occurs as radial aggregates of orange crystals. The results of XRD measurements show highly variable cell parameters, in agreement with published data (McDonald and Cruickshank 1967; Cooper et al. 1981; Libowitzky et al. 1997; Boni et al. 2003; Coppola et al. 2008). The *a* values vary between 8.336(6) and 8.363 (3) Å, while *b* ranges between 10.699(6) and 10.953(7) Å and *c* between 5.105(6) and 5.123(4) Å.

Goethite

XRD analyses revealed the presence of goethite in most nonsulfide specimens from the Silesia–Cracow province, in good agreement with the descriptions made by other authors (Zabinski 1960; Radwanek-Bak 1983) for whom goethite represents one of the most commonly occurring phases in the *red galman*. A common feature noticed in the specimens from the Boleslaw mine (i.e., CV05-51) is that Fe(hydr)oxides replace pyrite crystals along cleavage planes (Fig. 7d). Only in a few concretions consisting of pure smithsonite and hemimorphite, goethite seems to be absent. Locally, we also detected hematite.

Other minerals

Our investigation has confirmed the presence of cerussite, hydrocerussite, Zn-, Pb-, Fe-, and Mn-(hydr)oxides, as well as relics of sulfides. All these mineral phases have been mentioned in previous mineralogical studies (Zabinski 1960; Radwanek-Bak 1983; Gruszczyk and Wielgomas 1987; Smakowski and Strzelska-Smakowska 2005).

Calcite is the main gangue mineral and occurs in the entire mining province. It is usually a late phase that follows the deposition of most nonsulfide minerals in fractures and cavities. *Tarnowitzite* (a Pb-rich aragonite containing from 2.93% to 4.60% Pb, Czaja 1978) has been detected only in a single sample from the Trzebionka mine (CV05-55) (Fig. 5d). Minute chalcedony concretions have been detected only in few archival samples from the Matylda mine (CV05-73, CV05-74, CV05-75), where they are associated to Zn–dolomite.

Petrography and paragenesis

Two distinct mineral associations have been recorded in the Cracow–Silesia *galmans*:

1. smithsonite/hemimorphite/goethite—dominated nonsulfides:

This mineral association is typical of the Zn nonsulfide deposits of supergene origin worldwide. Local variations in the paragenesis have been detected: smithsonite is the dominant and older mineralogical phase, while hemimorphite is younger and less widespread compared to smithsonite. Hydrozincite, which was detected only in outcrop, as a thin veneer on the previously deposited phases (Fig. 5a), appears to be postdating late hemimorphite.

2. Fe–smithsonite/Zn–dolomite-dominated nonsulfides:

This paragenesis has been observed mainly in samples from the Matylda mine, but also occurs sporadically in other mines of the district. The minerals detected here do not generally occur in the typical supergene deposits.

Distinct generations of smithsonite, not always comparable throughout the entire mining district, have been observed in most analyzed samples. Smithsonite was classified based on morphology, following the methodology used for other nonsulfide deposits (Sardinia: Boni et al. 2003; Belgium: Coppola et al. 2008).

A first generation of microcrystalline smithsonite (type A, Fig. 6a,b) has been observed to replace both host dolomite (OBD I and II) as well as sphalerite. The partially replaced dolomitic host rock shows blotchy blue and red colors under cathodoluminescent light. Type A smithsonite is evenly distributed in the entire mining province. Younger smithsonite generations with different morphologies form concretions and crystalline aggregates in open cavities and fractures in the host rock. Peculiar concretions, consisting of globular zoned crystals (type B), have been observed in cavities and fractures of many samples from the Boleslaw open pit and the Trzebionka mine (Fig. 6a,c). Under CL, they usually show a blue-red luminescence in the crystal cores and a blue-pink zoned luminescence in the outer rim (Fig. 6b,d). Zoned rhombohedral crystals (type C), which probably represent one of the last smithsonite generations, grow in cavities. Typical C forms are the crystals observed in the specimens from the Bibiela dumps (Fig. 6e). The luminescence of type C smithsonite crystals varies from pale blue-pink in the core, to bright red at the rims (Fig. 6f). Zoned hexagonal crystals of smithsonite (type D), with a zoned blue-pink luminescence, grow both on the inner and on the external border of empty cavities of former saddle dolomite crystals (Fig. 6g and h). The peculiar pink luminescence of some smithsonite generations could be ascribed to a high Mn content in the crystal lattice (Götte and Richter 2004).

In the Boleslaw open pit, smithsonite occurs both in type A (Fig. 6a and b) and type D (Fig. 6g) morphologies. The size of the smithsonite crystals in type A is less than 100 μm, while in type D, the individuals can reach 400 μm in diameter. The same morphology has been observed also in the specimens collected from the dumps around Miasteczko Slaskie in the northwestern part of the district, a few kilometers north of Tarnowskie Gory.

Globular concretions of Zn-carbonates (type B), growing on and/or partly replacing several dolomite generations, have been observed in a few samples from the Boleslaw and Trzebionka mines (Fig. 6c and d). Rhomboedral crystals in cavities (type C) have been found in a few samples from the Bibiela dumps (Fig. 6e and f). Another smithsonite morphology (type E) has been recognized in a few specimens collected at Trzebionka. Type E smithsonite crystals (maximum size 700 μm) have a scalenohedral habit and occur as concretions in the empty cavities of OBD I.

Tabular crystals of clear hemimorphite may follow the last smithsonite generations growing in cavities and fractures (i.e., in the samples from Bibiela). However, hemimorphite can also grow directly in the hollow frames of the former dolomite crystals (as in the Boleslaw mine).

Several chemically distinct generations of Fe-bearing smithsonite have been recorded in the samples from the Matylda mine (Figs. 5e, 7a and b). The first generation occurs as subhedral crystals with a cryptocrystalline texture, replacing dolomite host rock. Under CL, this smithsonite shows variably blotchy red-blue luminescent to nonluminescent colors. A later generation of pure smithsonite, showing a zoned blue-pink luminescence grows in cavities

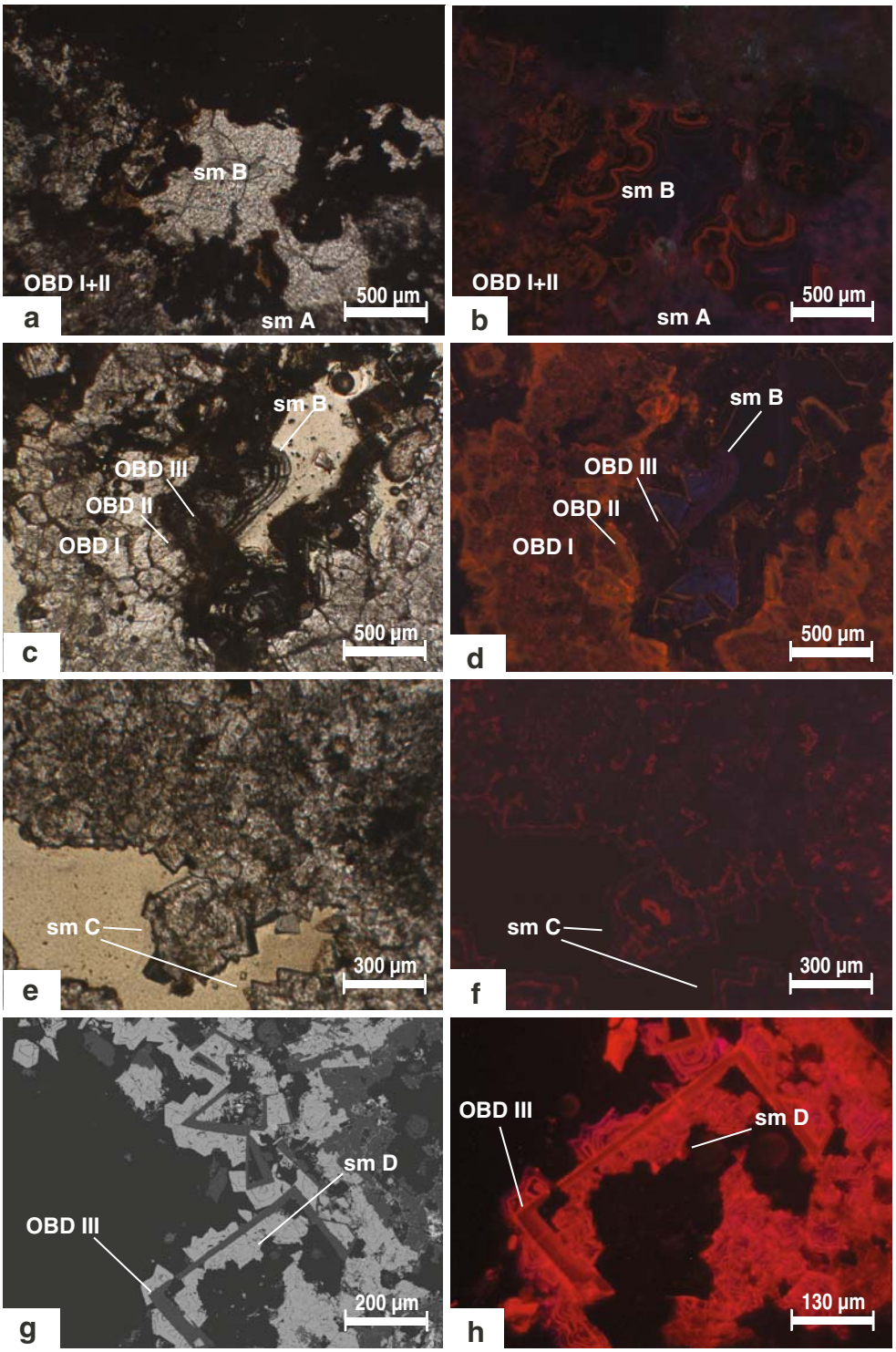

Fig. 6 **a**, **b** Dolomite host rock partially replaced by microcrystalline smithsonite (type A) with late smithsonite (type B) sealing voids and relicts of oxidized sulfides, Boleslaw deposit (CV05-58), thin section (NII); **b** CL image of (**a**); **c** Late smithsonite generation (type B) on OBD III, Boleslaw deposit (CV05-51b), thin section (NII); **d** CL image of (**c**); **e** Rhombohedral zoned crystals of smithsonite (type C) in a cavity, Bibiella dump (CV05-29), thin section (NII); **f** CL image of (**e**); **g** Zoned hexagonal scalenohedral crystals of smithsonite (type D) growing on the border of skeleton crystals of OBD III, Boleslaw deposit (CV05–51b), backscattered electron image; **h** CL image of (**g**);

and is followed by Fe-rich smithsonite. A single generation of Fe–smithsonite coexisting with smithsonite has been detected in a sample from the Bibiela dumps (i.e., CV05-28), where this phase occurs as solid inclusions in an earlier generation of Fe–dolomite (Fig. 7c). The fluid inclusion assemblage observed in the Fe–smithsonite from Matylda shows the predominance of monophase aqueous all-liquid inclusions.

Several generations of Zn-rich dolomite occur in the horizon II (Fig. 2) of the Matylda mine (sample CV05-73; Fig. 7f). According to previous authors (Zabinski 1960; Smakowski and Strzelska-Smakowska 2005), this dolomite,

associated to Fe–smithsonite, may be included in the mineralogical assemblage of the *white galman*, which is represented almost exclusively in this ore horizon (Kucha 2003, 2005). An early Zn-rich dolomite, (hydr)oxide-free, occurs as planar euhedral crystals in an idiotopic mosaic (*sensu* Sibley and Gregg 1987) with single crystal sizes of less than 200 μm. These are cemented by a later dolomite generation containing Fe–Mn(hydr)oxides (mainly goethite), occluding the porosity. In several open cavities, bigger crystals are visible (up to 500–600 μm), showing a clear external rim a few micrometers thick and (hydr)oxides bands, parallel to the crystal faces (Fig. 7f). Under cold CL microscopy, the earliest (hydr)oxide-free dolomite is less luminescent (dull red) than the later generations (bright red). However, it is impossible to distinguish between the clear external rims of the dolomite crystals occurring in cavities and the dolomite generation impregnated with Fe-(hydr)oxides, due to their similar luminescence colors.

Late calcite, syn- or post-nonsulfide emplacement, with orange cathodoluminescence colors, fills the remaining porosity, but it can also cut and/or locally replace the dolomitic host rock (Fig. 7d).

Major and trace element geochemistry of nonsulfide ores

Zinc in the Polish nonsulfide ores is contained preferentially in smithsonite, Fe–smithsonite, Zn–dolomite, and in minor abundance in hemimorphite, hydrozincite, Zn-sulfates (mainly goslarite) and in Mn-(hydr-)oxides, which contain a few thousand ppm Zn. Lead occurs in unweathered galena remnants and in alteration products, like cerussite and hydrocerussite. Chemical analyses (WDS) of the most important nonsulfide minerals in the district are shown in Table 2.

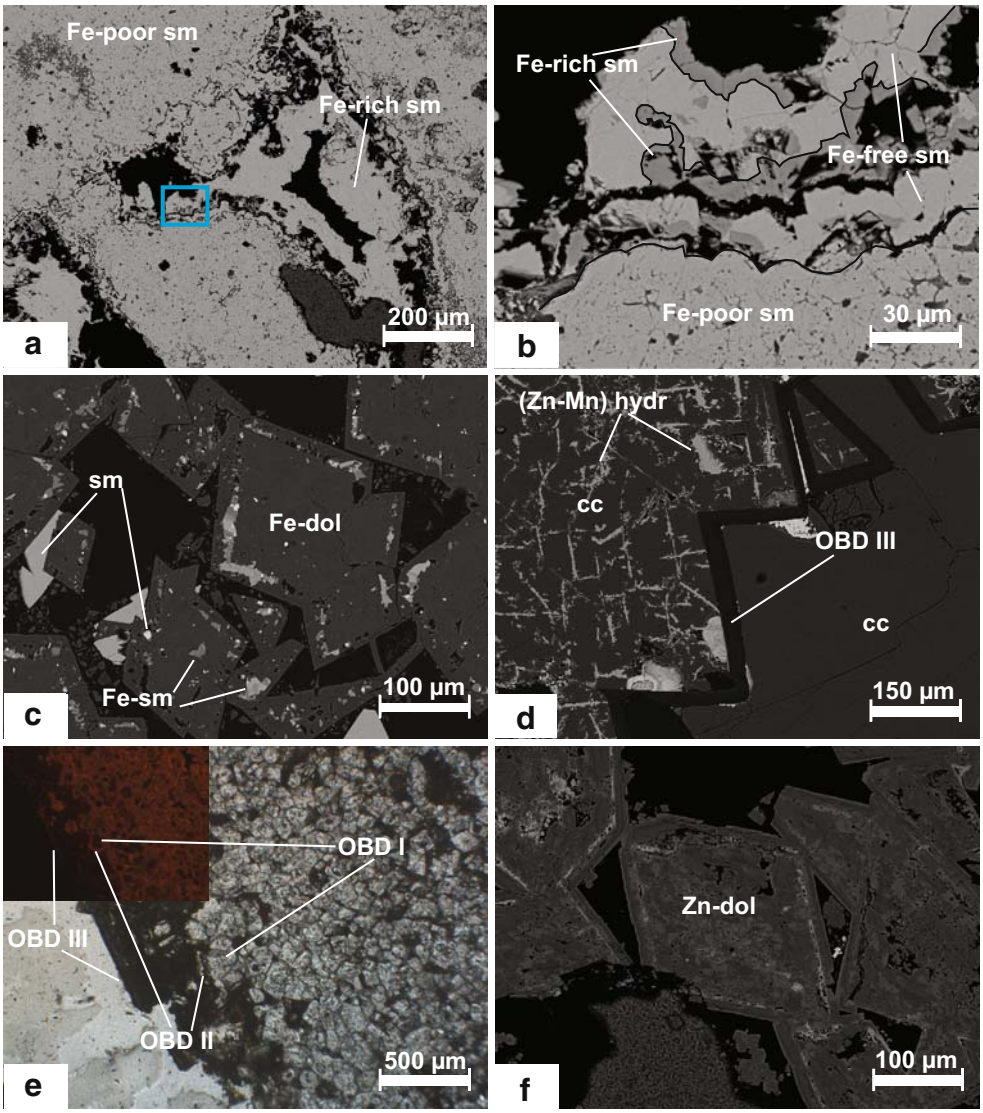

Fig. 7 **a** Microcrystalline Fe (poor)–smithsonite from *white galman*, with late smithsonite, and Fe(rich)–smithsonite in a cavity, Matylda mine (CV05-86), backscattered electron image; **b** enlargement of a selected area from (**a**) showing the relationships between three different types of smithsonite, Matylda mine (CV05-86); **c** Inclusions of smithsonite and Fe–smithsonite in the porosity of Fe–dolomite (OBD II), Bibiella dump (CV05-28), backscattered electron image; **d** Late calcite filling OBD III crystals with Zn–Mn (hydr-)oxides in the cleavage fractures, Boleslaw mine (CV05-51); **e** OBD III growing on OBD I (core crystals), cemented in turn by OBD II (rim crystals); Boleslaw deposit (CV05-50), thin section image (NII); CL image in the corner; **f** Rhomboedral crystal of Zn–dolomite (*white galman)*. The clear zones are Fe-rich and the darker ones Zn-rich; Matylda mine (CV05–73), backscattered electron image

Trace levels of metals were found associated with Zn in the crystalline structure of smithsonite. The MgO and CaO contents may reflect the presence of dolomite remnants not completely replaced by smithsonite. Traces of Mn, Co, and Ni have been detected in all analyzed smithsonite samples. Cadmium occurs in smithsonite only in traces, but in specimen CV05-80, where the Zn-carbonate is directly in contact with sphalerite, the CdO content is higher (Table 2).

Combined SEM and microprobe analyses have revealed the presence of Fe-rich smithsonite in few specimens from the Bibiela dumps and the Matylda mine. Fe–smithsonite was not detected by XRD, possibly due to concentrations below the detection limits. At Bibiela, solid inclusions of Fe–smithsonite inside former Fe–dolomite crystals contain up to 16.5 wt.% FeO and 2.5 wt.% MnO. In the Matylda mine, at least three generations of Fe–smithsonite have been detected. The first, most abundant generation (Fe-poor smithsonite) is cryptocrystalline. It contains up to 2 wt.% FeO and ≈60 wt.% ZnO. In the cavities of the Fe–smithsonite, a second smithsonite generation with only traces of FeO occurs, which is followed by another generation of Fe-rich smithsonite. The FeO and ZnO contents of the latter generation are constrained between 15.4 and 16.8 wt.% FeO and 32.9 to 34.9 wt.% ZnO, respectively.

A combined SEM-WDS study, carried out on several dolomite specimens from different mines, has confirmed the presence of a first dolomite generation (OBD I) with a nearly stoichiometric composition and a limited Zn content (up to 0.7 wt.% ZnO). Iron can reach concentrations up to 0.7 wt.% FeO in this dolomite, and Mn up to 0.2 wt.% MnO; other metals have been detected only in traces. The second dolomite type (OBD II) has a slightly higher FeO

Table 2 WDS analyses of selected smithsonite, Fe–smithsonite, hemimorphite, cerussite, and dolomite samples from the Silesia–Cracow district (S Poland), pointing to compositional variations

Sample															
Smithsonite and Fe–smithsonite															
	CV05-15			CV05-56			CV05-86			CV05-80			CV05-28		
ZnO	61.34	60.18	64.41	62.31	60.68	60.77	60.47	60.83	62.07	59.10	58.07	59.28	61.53	62.56	38.02
FeO	0.56	3.15	0.35	tr	n.d.	0.43	0.72	1.86	1.14	tr	tr	tr	0.85	0.28	16.50
MnO	Tr	n.d.	tr	n.d.	n.d.	n.d.	tr	tr	tr	tr	tr	n.d.	tr	tr	2.49
CaO	1.13	0.76	1.07	0.86	1.18	1.12	0.91	0.37	0.27	1.04	0.14	1.15	0.79	0.79	2.65
MgO	1.20	0.34	0.14	0.63	0.67	0.75	1.42	0.56	0.31	tr	0.14	0.10	0.48	0.48	2.03
CdO	Tr	tr	tr	tr	0.77	0.60	tr	0.30	tr	2.84	4.19	1.87	0.17	0.12	n.d.
PbO	Tr	n.d.	tr	0.54	1.06	0.85	tr	tr	tr	0.95	1.11	1.36	0.66	0.66	0.17
CO_2*	35.96	35.97	36.22	35.30	35.15	35.41	36.13	36.45	36.10	34.18	34.30	34.10	35.31	35.31	35.39
total	100.19	100.40	102.19	99.64	99.51	99.93	99.65	100.37	99.89	98.11	97.95	97.86	99.79	100.20	97.25

	Cerussite					Hemimorphite								
	CV05-56		CV05-80			CV05-14			CV05-24			CV05-27		
ZnO	0.30	0.28	0.23	1.13	SiO_2	26.45	26.24	26.79	25.85	25.75	25.47	26.59	26.52	26.49
FeO	tr	n.d.	n.d.	n.d.	ZnO	66.91	66.89	67.3	65.73	66.79	66.86	65.69	65.78	65.49
MnO	tr	tr	n.d.	n.d.	FeO	tr	0.09	0.20	0.13	0.10	0.12	0.014	0.019	n.d.
CaO	0.26	0.19	0.85	0.63	CaO	0.04	0.06	0.00	0.07	0.02	0.04	0.35	0.43	0.46
PbO	82.40	82.67	82.12	81.09	PbO	n.d.	tr	n.d.	0.07	0.09	0.07	0.46	0.28	0.35
CO_2*	16.85	16.73	17.17	17.25	H_2O*	6.63	6.81	5.68	8.01	7.25	7.35	6.95	6.96	7.23
Total	99.81	99.87	100.37	100.10	Total	100.03	100.09	99.98	99.85	99.99	99.91	100.05	99.99	100.02

Zn-poor dolomite (OBD I and II), Zn-rich dolomite (OBD III & dolomite from Matylda mine), Fe-dolomite															
	OBD I			OBD II			OBD III			Matylda mine				Fe-dol	
	CV05-15			CV05-15			CV05-51			CV05-73				CV05-28	
ZnO	0.27	0.1	0.69	0.44	0.85	0.17	1.27	1.65	2.54	5.47	5.39	2.01	3.56	0.03	0.04
FeO	0.65	tr	0.16	0.3	1.14	1.26	0.14	0.29	0.2	1.28	0.2	3.01	0.12	7.32	10.82
MnO	0.15	0.21	0.13	0.13	0.13	0.17	0.27	0.14	0.06	0.71	0.58	0.61	0.60	0.83	1.29
CaO	31.07	30.73	31.22	31.13	31.74	31.56	32.5	31.34	31.75	28.56	29.2	29.27	29.27	30.62	28.62
MgO	20.03	21.09	20.62	19.95	18.77	19.01	18.72	19.01	19.37	17.06	17.22	17.85	19.48	15.45	13.62
PbO	n.d.	n.d.	n.d.	n.d.	n.d.	n.d.	0.04	n.d.	0.08	n.d.	0.11	0.07	tr	n.d.	n.d.
CO_2[a]	48.05	47.48	47.9	46.93	46.75	46.61	47.01	46.62	47.72	45.32	47.4	46.14	46.96	46.04	45.06
Total	100.2	99.61	100.7	98.88	99.38	98.78	99.95	99.05	101.7	98.40	100.10	98.96	99.99	100.3	99.45

tr content in traces, *n.d.* not determined

[a] Calculated from stoichiometry

(between 0.3 and 1.3 wt.%) and ZnO (between 0.2 and 0.9 wt.%) content. The latter type occurs throughout the entire district, except in the specimens from the Matylda mine. The paragenetically subsequent dolomite generation (OBD III) has a much higher Zn content (up to 2.5 wt.% ZnO) with respect to OBD I and II, while Fe is very low (0.1–0.3 wt% FeO). An exceptionally Fe-rich dolomite variety was observed only in the sample CV05-28 from the Bibiela dump. This dolomite type is nonluminescent under CL, due to the Fe-quenching effect or to possible self-quenching by high Mn concentrations (Machel et al. 1991).

The dolomite from the ore horizon II in the Matylda mine (CV05-73) is somewhat different. Its Zn content is the highest detected in the dolomites of the whole district (between 3.3 and 5.5 wt.% ZnO), while Fe has a variable content between 0.1 and 3 wt.% FeO, randomly distributed in the crystal lattice.

Carbon and oxygen isotopes

To calculate the formation temperatures and characterize the fluid type, it is necessary to determine the oxygen isotopic composition of the carbonate minerals and their parent fluids, as well as to use appropriate equations to model the isotopic fractionation (Gilg et al. 2008). In the supergene environment, these temperatures are correlated to the mean air temperature and climate. Stable isotope (O–C) geochemistry was carried out on smithsonite, cerussite, aragonite, and calcite specimens from several nonsulfide deposits. Results are presented in Table 3 and in Fig. 8.

Smithsonite

We have measured the carbon and oxygen isotopic ratios of smithsonite in the *red* and *white galman* types, sampled in several mines throughout the district (Fig. 8).

The difference between *white* and *red galman* ore types is mirrored by the stable isotope results obtained from the Zn-carbonates. Smithsonite from *red galman* shows a limited range of $\delta^{13}C_{VPDB}$ values (−10.1‰ to −11.4‰, 1σ=0.16, n=11) and slightly variable $\delta^{18}O_{VSMOW}$ values (25.3 to 28.5‰, av. 26.8±0.3‰, 1σ=0.28, n=11). However, the low uniform values of $\delta^{13}C_{VPDB}$ detected in this type of smithsonite are unusual for supergene nonsulfide Zn deposits (Boni et al. 2003; Coppola et al. 2008; Gilg et al. 2008). They indicate the predominance of a single, reduced and possibly soil-derived, carbon source during the formation of *red galman* smithsonite. Smithsonites from *white galman* have more variable and positive carbon isotope values (−2.9‰ to −7.4‰) than those from *red galman*, but broadly similar oxygen isotope compositions (26.8‰ to 28.9‰). The slight variation in $\delta^{18}O_{VSMOW}$ (~3‰ "*red galman*" smithsonite, ~2‰ "*white galman*" smithsonite) could be due to a change in isotopic composition of the fluid and/or to temperature variation during precipitation, which is very common for supergene deposits (Boni et al. 2003; Gilg et al. 2008). The C-isotope range of the *white galman* smithsonite, commonly reported in supergene smithsonites worldwide (Gilg et al. 2008), indicates a mixed contribution of carbon derived from the OBD host rocks and organic carbon from the soil or oxidized bacteria. No correlation was found between stable isotope values and

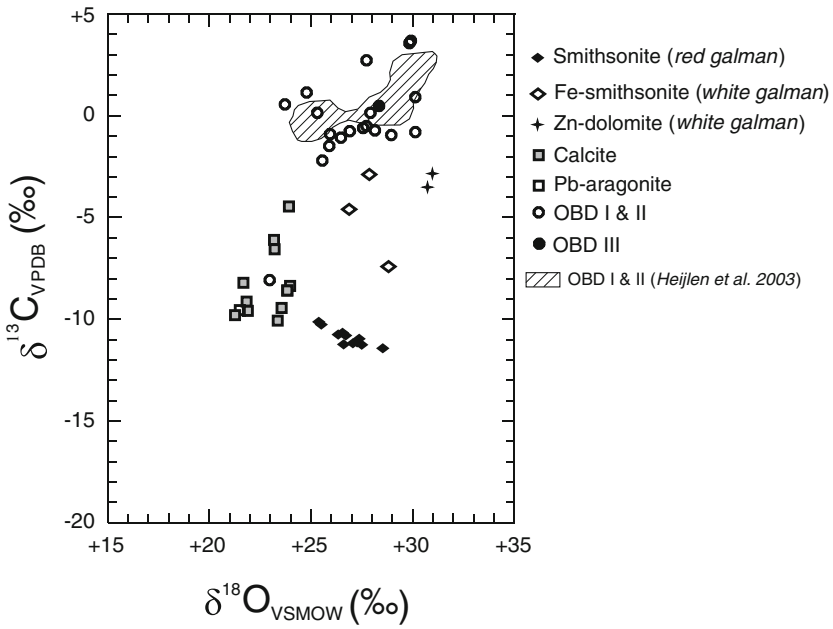

Fig. 8 Plot of $\delta^{13}C$ vs. $\delta^{18}O$ for various Zn, Ca, and Mg–Ca carbonates (smithsonite, supergene calcite/aragonite and dolomite generations OBD I, II, III) from Polish nonsulfide ores

Table 3 Carbon and oxygen isotope data of Zn, Ca, and Mg–Ca carbonates from the Silesia–Cracow district (S Poland)

Sample	Mineral*	Description	Location	$\delta^{13}C_{V\text{-}PDB}$ (‰)	$\delta^{18}O_{V\text{-}SMOW}$ (‰)	Ave	$\pm\sigma$
CV05-27b	sm	Massive crystalline smithsonite	Bibiella	−10.8	26.3		
CV05-27a	sm	Aggregates of brown crystals	Bibiella	−10.8	26.6		
CV05-30a	sm	Fragmented and altered crystalline smithsonite	Bibiella	−11.2	27.0		
CV05-30b	sm	Massive crystalline smithsonite	Bibiella	−11.1	26.6		
CV05-32a	sm	Massive crystalline smithsonite	Bibiella	−10.8	26.7		
CV05-32c	sm	Rhombohedral red crystals in cavities	Bibiella	−11.1	27.3		
CV05-33a	sm	Cariated crystalline smithsonite	Bibiella	−11.0	27.4		
CV05-56a	sm	Crystalline concretion, outer part	Tzrebionka	−10.1	25.3		
CV05-56b	sm	Crystalline concretion, inner part	Tzrebionka	−10.2	25.4		
CV05-82a	sm	Earthy reddish matrix	Tzrebionka	−11.4	28.5		
CV-71B	sm	Globular vitreous concretion	Matylda	−11.3	27.5	26.8	0.9
CV05-64b	Fe–sm	Brown crystalline aggregates (*white galman*)	Olkusz	−4.7	26.8		
CV05-63a	Fe–sm	Massive crystalline smithsonite (*white galman*)	Matylda	−7.4	28.9		
CV05-85b	Fe–sm	Spherical crystalline aggregates (*white galman*)	Matylda	−2.9	27.8	27.8	1.0
CV05-73a	Zn-rich dol	White concretion in cavity	Matylda	−3.5	30.8		
CV05-73b	Zn-rich dol	Massive microcrystalline host rock	Matylda	−2.9	31.0	30.9	0.2
CV05-50a	dol (OBD I)	Massive gray host rock	Boleslaw	−1.4	26.0		
CV05-9b	dol (OBD I–II)	Massive gray host rock in clasts	Boleslaw	−0.7	27.0		
CV05-51Ba	dol (OBD I)	Massive gray host rock in clasts	Boleslaw	−0.9	26.0		
CV05-51b	dol (OBD I–II)	Massive gray host rock	Boleslaw	−8.0	23.0		
CV05-44a	dol (OBD I–II)	Massive gray host rock	Boleslaw	−2.3	25.5		
CV05-79b	dol (OBD III)	Reddish rhombohedral crystals in cavities	Boleslaw	−7.9	22.9		
CV05-15a	dol (OBD I–II)	Massive gray host rock in clasts	Boleslaw	−0.5	27.8		
CV05-11c	dol (OBD I–II)	Spherical crystalline aggregates	Boleslaw	0.3	28.0		
CV05-17a	dol (OBD I–II)	Laminated sediment	Boleslaw	−0.8	30.1		
CV05-2a	dol (OBD I–II)	Massive wall rock	Boleslaw	0.9	31.1		
CV05-44b	dol (OBD III)	Reddish rhombohedral crystals in cavity	Boleslaw	0.6	28.3		
CV05-49a	dol (OBD I–II)	Massive microcrystalline host rock	Boleslaw	−1.0	26.4		
CV05-35a	dol (OBD I)	Microcrystalline host rock	Bibiella	0.5	23.7		
CV05-54b	dol (OBD I–II)	Massive microcrystalline host rock	Bytom	−0.5	27.6		
CV05-74b	dol (OBD I)	Massive microcrystalline host rock	Matylda	0.2	25.3		
CV05-75a	dol (OBD II)	Microcrystalline host rock	Matylda	1.1	24.8		
CV05-25a	dol (OBD I–II)	Residual sediment granulometrically homogeneous	Pomorzany	2.8	27.7		
CV05-25b	dol (OBD I–II)	altered red dolomite	Pomorzany	3.6	29.8		
CV05-25c	dol (OBD I–II)	Yellow altered dolomite in clasts	Pomorzany	3.6	29.9		
CV05-25d	dol (OBD I–II)	Gray dolomite matrix	Pomorzany	−0.7	28.2		
CV05-20a	dol (OBD I–II)	Rubefied dolomite	Tzrebionka	−1.0	28.9	27	2.324
CV05-68a	ce	White crystals	Olkusz	−12.8	13.8		
CV05-6a	cc	White crystals	Boleslaw	−4.4	23.9		
CV05-60a	cc	Rhombohedral white crystals on sulfides	Boleslaw	−9.8	21.4		
CV05-78b	cc	Globular white vitreous concretion	Boleslaw	−8.7	23.8		
CV05-77b	cc	white vitreous concretion	Boleslaw	−6.6	23.2		
CV05-45b	cc	White crystals	Boleslaw	−6.1	23.2		
CV05-34b	cc	White vitreous concretion	Boleslaw	−9.4	23.5		
CV05-8a	cc	Red crystals in cavities	Boleslaw	−10.1	23.3		
CV05-51a	cc	Calcite in veins	Boleslaw	−8.4	23.9		
CV05-55b	cc	Crystalline massive level	Tzrebionka	−9.6	21.9		
CV05-55a	cc	Fibrous white crystals	Tzrebionka	−8.2	21.7		
CV05-55b	Pb–Ar	Crystals layer	Tzrebionka	−9.5	21.5		
CV05-24a	cc	Globular white vitreous concretion	Pomorzany	−9.2	21.8	22.8	1.01

[a] *cc* calcite, *ce* cerussite, *dol* dolomite, *Pb–Ar* Pb–aragonite, *sm* smithsonite

smithsonite morphology and/or chemistry, as reported in other supergene deposits (Boni et al. 2003).

Calcite

Late calcite shows a very restricted range of $\delta^{18}O$ values between 21.3‰ and 23.9‰ (av. 22.8±1.5‰, 1σ, n=12). The C-isotope values have a wider spread, but are all distinctly negative (−4.4‰ to −10.1‰). Pb–aragonite (specimen CV05-55B) has a stable isotopic composition ($\delta^{13}C$=−9.5‰ and $\delta^{18}O$=21.5‰) comparable with that of meteoric calcite. The data show a predominance of the light C-source (organic matter) during the precipitation of both calcite and aragonite. However, the most ^{13}C-enriched calcite (−4.4‰) has been detected in the sample CV05-6 from Boleslaw mine, where nonsulfides are absent. This sample can represent a calcite deposited in a barren zone, not directly precipitated by metal-bearing fluids.

The $\delta^{18}O$ ratios of calcites are about 4‰ lower than those of the supergene smithsonites, thus compatible with a meteoric origin, and are in accord with the theoretical model of isotope fractionation between carbonate minerals and water proposed by Gilg et al. (2008).

Dolomite (OBD I, II, III)

It was impossible to separate OBD I from OBD II for isotopic analysis, due to the tight intergrowth of both generations. The measured samples therefore generally consist (with few exceptions) of both generations OBD I and OBD II. Mixed OBD I and II samples show $\delta^{13}C_{VPDB}$ values ranging from −2.25‰ to 3.62‰ (av. 0.17‰, 1σ= 1.68) and $\delta^{18}O_{VSMOW}$ values constrained between 23.7‰ and 31.1‰ (av. 27.4‰, 1σ=2.03). These values are comparable with stable isotope results on bulk samples of OBD I and II from the Trzebionka and Pomorzany area obtained by Heijlen et al. (2003; Fig. 8) and with the values of OBD from the Pomorzany area published by Narkiewicz (1993), where no distinction was made between OBD I and II. Very low values for both $\delta^{13}C$ (−8.1‰) and $\delta^{18}O$ (22.9‰) have been recorded in the CV05-51B dolomite sample (Boleslaw mine). The relatively low $\delta^{13}C$ values could be caused by the presence of late meteoric calcite in microveins, as evidenced by petrography. Meteoric calcite shows relatively negative values of $\delta^{13}C_{VPDB}$ in the supergene environment (Cerling 1984; Yapp 1997; Gilg et al. 2008) and could have contributed to the ^{13}C-poor imprint of the dolomite. Carbon and oxygen isotopic compositions of a single OBD III sample show values comparable with those of the previous dolomite generations.

A Zn-rich dolomite sample (this term refers to dolomite with high Zn content of up to 6% ZnO and has here no genetic meaning) from the Matylda mine (sample CV05-73) is slightly depleted in ^{13}C (−3‰) compared to other dolomite generations. This may point to a major contribution of a C-reduced source during precipitation of Zn–dolomite at Matylda and may be evidence of a genetic mechanism different from that of the other dolomites. Also, the oxygen isotope ratios of the Matylda dolomite are ~3‰ higher (30.8‰) than in the other dolomite generations.

Discussion and conclusions

Geological factors controlling the formation of the Polish supergene nonsulfide deposits

Literature data and field observations at the deposit scale suggest that several factors played a key role in nonsulfide mineralization in the Silesia–Cracow district. The most important are:

1. Reactivation of old tectonic lineaments and intense block faulting.

According to Heijlen et al. (2003), the tensional tectonic regime established in the Silesia–Cracow district during the Cretaceous was the driving force for primary sulfide mineralization. If the primary Zn–Pb mineralization was formed in the Early Cretaceous, as evidenced by Rb–Sr sphalerite dating, then the uplift and block-faulting processes, which continued to affect these areas also during Tertiary, were able to cause the dislocation of the carbonate lithotypes hosting the sulfide ores to a near-surface environment, thus rendering them more vulnerable to the action of meteoric waters. The combination of generalized uplift and *horst*-and-*graben* tectonics was controlling the deep oxidation of sulfides and concomitant supergene nonsulfide formation. The acting mechanisms were twofold: (a) dislocation of the blocks hosting the primary sulfide ores up to higher morphological levels, and (b) creation of conduits preferentially along the fault directions for meteoric fluids to infiltrate. The main fault network with both N–S and E–W directions is supposed to have been produced in this region during the late Alpine phase (Tertiary; Gorecka 1993; Leach et al. 1996).

2. Effect of impermeable levels (especially the Keuper claystone) acting as impervious barriers.

The local presence of impermeable Keuper sediments on the top of OBD lithotypes hosting the primary sulfide deposits protected them from an intensive percolation of oxidized meteoric waters and therefore from weathering effects. Evidence exists in the Boleslaw area, where supergene nonsulfides mainly occur in the *horst* blocks, where Keuper sediments are absent or have a reduced

thickness. On the contrary, supergene ores are only seldomly reported from the *grabens*, where the cover of the Keuper claystone is still very thick (Fig. 2a). The situation is again quite different in other areas, as in Chrzanów region, where primary ore deposits (sulfides and *white galman*) were partially protected by Jurassic sedimentary rocks located on top of the OBD (Fig. 2b).

3. Presence of a network of karst cavities filled by sulfide-mineralized breccias.

The uplift processes linked to the final stages of the Alpine orogeny have promoted the lowering of the groundwater table, thus favoring the formation of a deep karstic network with a well-developed vadose zone (Cabala 2001).

4. Irregular porosity and permeability of the host rock.

The different OBD generations have a very irregular, locally interconnected porosity. The fault system, together with the fractures derived from the reactivation of preexisting basement faults, greatly enhanced the permeability of the carbonate rocks, thus favoring circulation of the oxidized metal-bearing fluids and supergene alteration of sulfides (Cabala 2001).

5. Buffer role played by both dolomite and limestone on the acid, metal-carrying fluids derived from sulfide oxidation.

Stable isotopes of supergene nonsulfide deposits

The oxygen isotopic values for smithsonites from the Polish *galman* are very similar to those measured in other supergene smithsonites around the world (Boni et al. 2003; Coppola et al. 2008; Gilg et al. 2008). Similar $\delta^{18}O$ values were detected in smithsonite of both *red* and *white galman*, despite the hypothesized hydrothermal origin of the latter. A slightly larger spread (3.5‰) is recorded in the oxygen isotopic composition of *red galman* smithsonite compared to *white galman*. This variability can be related either to a change in the isotope composition of the fluid, to temperature changes or a combination of both. The measured values in smithsonite from *white galman* are more uniform and point to a constant composition and temperature of the fluid during the mineralizing process.

The fluid responsible for supergene oxidation of sulfides (and hence for *red galman* formation) is likely of meteoric origin. On the basis of most geological considerations (Migoń and Lidmar-Bergström 2001), the paleoweathering phenomena responsible for the oxidation of primary sulfides in the Silesia–Cracow area and the formation of *red galman* occurred between the Late Cretaceous and the Middle Miocene. Gilg (2003) calculated the H–O composition of paleometeoric water from three supergene kaolinite deposits in Lower Silesia, Late Cretaceous to Tertiary in age, at about −8‰ (VSMOW). Using the measured oxygen isotope composition of smithsonite and the paleometeoric water composition, we have calculated formation temperatures of about 7°C to 18°C for the Zn-bearing carbonates in the Silesia–Cracow mining province (Fig. 9). These temperatures are in agreement with a continental near-surface environment in a temperate climate. Moreover, they are similar to the temperatures measured in Belgian smithsonites, but slightly lower than the temperatures measured for supergene Zn deposits of Bavaria (Freihung) and southern Europe, as in the Iglesiente (SW Sardinia) and at Vila Ruiva (Portugal), which are 20°C±6 (Gilg et al. 2008). Also, the precipitation temperatures for late calcite (11–21°C) of meteoric origin in the Silesia–Cracow district are typical of a temperate climate.

Red galman smithsonite is ^{13}C-depleted and of uniform carbon isotope composition (−10.1‰ to −11.4‰). A similar range of values has been detected so far only in the supergene smithsonites at Villa Ruiva, Portugal (Gilg et al. 2008). The negative values indicate predominant C3 vegetation in the soils covering the deposits. The predominance of isotopically light, soil-derived carbon, with respect to atmospheric- and host rock-derived (including OBD I and II) carbon is a typical characteristic of the Polish *galman* ores. This is different from the situation in other supergene nonsulfide deposits, where a mixed (^{13}C-enriched and ^{13}C-depleted) carbon source has been detected in Zn-carbonates (Boni et al. 2003; Coppola et al. 2008; Gilg et al. 2008). Also, calcite associated to *red galman* mineralization has a very variable but still negative C-

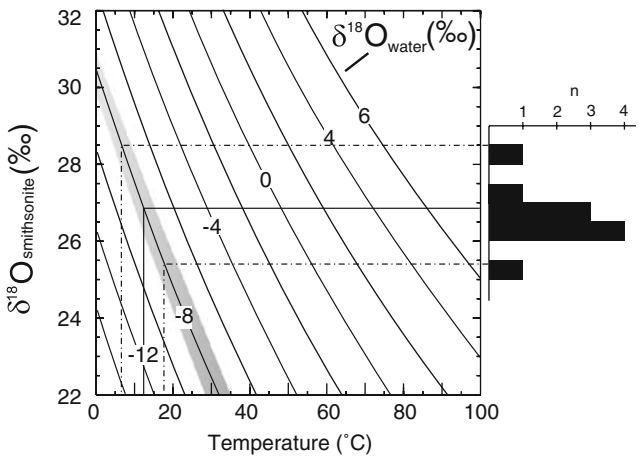

Fig. 9 Graphical representation of oxygen isotope equilibrium curves between smithsonite (*red galman*) and water according to Gilg et al. (2008), calculated for different $\delta^{18}O_{water}$ values as a function of temperature. The histogram to the right shows the oxygen isotope composition of smithsonite in *red galman* from the Upper Silesia district. Calculated temperatures for smithsonite formation are based on the $\delta^{18}O$ value of −8.0±1.0‰ for the local paleometeoric water as proposed by Gilg (2003). Note: *dashed line* maximum and minimum $\delta^{18}O$ values, *continuous line* average $\delta^{18}O$ values

isotope composition (approximately −8‰), which points to a predominance of the ^{13}C-depleted source in the precipitation of calcite as well.

It is possible that at least part of the sulfide dripstones (made of sphalerite and marcasite), and the unconsolidated brunckite occurring in the Trzebionka mine may have been deposited under reducing conditions in the cementation subzone below the *galman* carbonates and oxides. Such a setting is the case of the supergene sulfides in the *gossan* at the Broken Hill mine, New South Wales (Lawrence and Rafter 1962) or in the VHMS deposits of the southern Urals (Belogub et al. 2008). In both examples, the supergene sulfides have strong negative $\delta^{34}S$ values, possibly derived from the interaction with the soil-derived organic matter, as in the Upper Silesian speleothemes as well (as low as −37% $\delta^{34}S$; Leach et al. 1996).

Origin of white galman

Nature, origin, and distribution of *white galman* are still highly uncertain, since all occurrences of *white galman* have been mined out, and literature data on this subject are scarce (Zabinski 1960). However, *white galman* is quantitatively negligible compared with the high tonnage of *red galman* exploited in the Cracow–Silesia district. Ferrous smithsonite and Zn–dolomite have been described as the main components of *white galman*, as typified in the Matylda mine, where sulfides are almost totally absent (Zabinski 1960; Kucha 2005).

In the literature, the *white galman* is commonly considered as either a by-product of the same hydrothermal event depositing the sulfide ores (Zabinski 1958, 1986; Panek and Szuwarzynski 1974; Bak and Nieć 1978) or a carbonate phase preceding the diagenetic precipitation of sulfides (Kucha 2005; Kucha and Czajka 1984). The stratigraphic position of the *white galman* at Matylda, which is equivalent to the position of sulfide horizons in the nearby Tzrebionka mine, has been generally quoted as support of the hydrothermal theory. After Zabinski (1960), the metasomatic overprint of the OBD host rock by Zn- and Fe-rich fluids was responsible for *white galman* formation. According to Kucha (2005) and Kucha and Czajka (1984), a carbonate stage with formation of Zn- and Fe-rich dolomite and smithsonite occurred in a sulfide-free reducing environment and preceded the primary sulfide mineralization. This metasomatic overprint could have been responsible for the formation of the smithsonite–siderite halo around the sulfide orebodies in the Trzebionka mine (Kucha 2003) and of the Fe–smithsonite–barite halo in the Boleslaw mine (Bak 1993).

Our study has evidenced the substantial mineralogical and geochemical difference between the samples representing *red* and *white galmans*. Goethite and hematite, ubiquitous in *red galman*, are absent in the *white galman* samples. However, the most crucial feature of *white galman* is the association of Fe–smithsonite and Zn–dolomite, which reflects the more reducing conditions compared to *red galman* ores. Fe–smithsonite from *white galman* has broadly similar oxygen isotope composition (26.8‰ to 28.9‰) as the smithsonite in *red galman*. The slight variation in $\delta^{18}O$ (~2‰) between the two types could be due to a variation in isotopic composition of the fluid and/or to temperature variation during Fe–smithsonite precipitation. The oxygen isotope ratios of the Zn-rich dolomite in *white galman* are ~3‰ higher (31‰) than in the other OBD samples. The same dolomite is slightly more depleted in ^{13}C (−3‰) compared to the other OBD generations.

If we consider the *white galman* (Fe–smithsonite and Zn–dolomite association) as a lateral facies formed during the primary hydrothermal event that precipitated both OBD II and sulfides, we must assume that the precipitation of both carbonate minerals was related to a fluid with the same characteristics as those associated with the primary mineralization event. Therefore, on the basis of the oxygen isotope composition (0 ‰) of the fluid that precipitated OBD II (Heijlen et al. 2003), we were able to calculate a temperature of precipitation for Fe–smithsonite and Zn–dolomite of 35–53°C (Fig. 10) and 30–38°C, respectively. The monophase fluid inclusions observed in the Fe–smithsonite from Matylda also confirm that this carbonate phase formed under relatively low-temperature conditions of less than about 50°C (Goldstein 2001). After Kozlowski (1995), homogenization temperatures of fluid inclusions in sphalerite from the primary ore deposits range from 40°C to 160°C. Assuming a maximum burial depth of 500 m, this

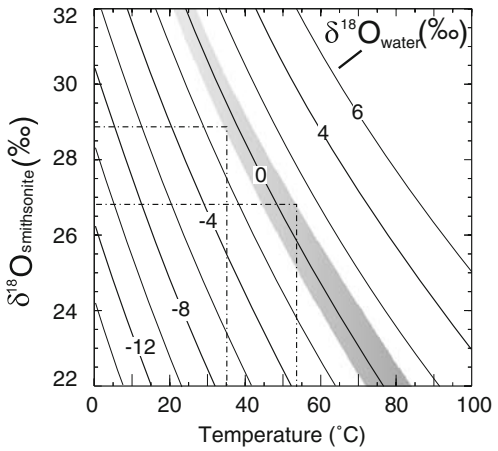

Fig. 10 Graphical representation of oxygen isotope equilibrium curves between smithsonite from *white galman* and water according to Gilg et al. (2008), calculated for different $\delta^{18}O$ water values as a function of temperature. Calculated temperatures for smithsonite formation are based on the $\delta^{18}O$ value constrained between −0.8 to +0.8‰ for the hydrothermal fluid as proposed by Heijlen et al. (2003). Note: *dashed lines* = maximum and minimum $\delta^{18}O$ values

variability reflects a thermal gradient related to fluid mixing and not to conductive heat loss (Leach et al. 1996). Both Fe–smithsonite and Zn–dolomite could have been deposited in the lower temperature range of this hydrothermal system, corresponding to the peripheral zones. The fact that Fe–smithsonite, siderite, and Zn–Fe–dolomite form halos of variable thickness around the main ore bodies (Gürich 1897; Bak 1993; Kucha and Czajka 1984) confirms the assumption that the *white galman* association formed in the low-temperature stage of the primary hydrothermal system. Zinc was precipitated as carbonate instead of sulfide from a sulfur-free fluid as suggested by Kucha (2005).

However, we cannot completely exclude a supergene origin for the *white galman* in the reduced zone of the weathering profile. If this would have been the case, then we should assume the same isotopic composition of Tertiary paleometeoric water as in the case of *red galman*, thus obtaining precipitation temperatures between 5°C and 12°C for both Fe–smithsonite and Zn–dolomite. These temperatures are similar (even if slightly lower) to those of *red galman* smithsonite.

Reichert and Borg (2008) give a completely different explanation for the differentiation between "red" and "white" Zn nonsulfide ores, detected in several Iranian deposits. These authors relate the different color of the ore types to distinct stages of metal refining and fractionation. The proximal "red" ores formed early in situ by sulfide oxidation, while the "white" ores are peripheral, late replacements of carbonate host rocks. This model is based on the iron oxide–smithsonite association in the "red" ore and smithsonite–hydrozincite in the "white" ore. The *white galman* of the Polish nonsulfides, instead, consists of Fe–smithsonite and Zn–dolomite, a mineral association that is quite different from the smithsonite–hydrozincite assemblage mentioned by Reichert and Borg (2008) for the Iranian "white zinc" ore.

Timing of polish nonsulfide Zn deposits

As discussed above, most (or all) of the Polish nonsulfides are supergene in origin (*red galman*) and represent the product of oxidation of primary sulfides derived from weathering and/or paleoweathering events. Only the so-called *white galman* may be genetically related to an earlier hydrothermal phase.

Both lower and upper temporal boundaries of supergene nonsulfide formation in Poland are currently uncertain. Age constraints on the genesis of these ores would also be of great importance to set an upper temporal limit to primary sulfide mineralization, which is still a much-debated question (Sass-Gustkiewicz et al. 1982; Leach et al. 1996; Heijlen et al. 2003). It is commonly agreed that the most favorable conditions for deep weathering processes existed in Poland from Early Tertiary to Middle Miocene (Dubinska et al. 2000; Migoń and Lidmar-Bergström 2001; Migón 2007). During this period, an extensive subaerial exposure facilitated the removal of parts of the Mesozoic and Tertiary cover, thus enabling the circulation of meteoric waters and the alteration of primary sulfides and of their host rocks. Erosion surfaces intersected by sinkholes and karstic channels are quite common in the region. Some of these channels are filled by Paleogene continental sediments, containing *galman* fragments (Szuwarzynski 1978; Fig. 3). Other karstic sinkholes occurring in the OBD and underlying the Gogolin Limestone also contain several fragments of nonsulfide ores embedded within continental sandy and clayey sediments of Paleogene age, under a cover of Tortonian marine sandy claystone (Gürich 1897; Panek and Szuwarzynski 1975; Szuwarzynski 1978; Fig. 3). It seems, therefore, probable that the main paleoweathering stage, responsible for the formation of most supergene Zn–(Pb–Fe) deposits in the Silesia–Cracow district, has taken place shortly before or during Palaeogene or Early Neogene. Block faulting induced by the late stages of the Alpine orogeny in the Early Tertiary could have contributed to enhance the circulation of meteoric fluids and the oxidation of primary sulfides before the Miocene marine ingression.

Other paleoweathering records with related saprolite deposits have been detected throughout the region: they could also help to constrain the age of the events responsible for the secondary Zn ores. Different ages have been attributed to the saprolite deposits occurring below a cover of Miocene sediments, but the most important of them seem to be of Early Tertiary age (Alexandrowicz 1969; Kowalski et al. 1979). At Szklary near Zabkowice Slaskie (Lower Silesia), about 200 km W of Cracow, a residual weathering mantle containing Ni–laterites and considered to be Palaeogene in age, was developed on serpentinites belonging to the Lower Paleozoic basement (Ostrowicki 1965; Niskiewicz 2000; Dubinska et al. 2000).

In conclusion, the formation of most nonsulfide ores in the Silesia–Cracow district (*red galman*) is the result of supergene weathering processes acting mainly during the Early Tertiary. A Tertiary age was also indirectly confirmed by the similarity of the O-isotopic signature of the paleometeoric waters deduced from *red galman* smithsonite (−8‰ VSMOW) with meteoric fluids forming the supergene kaolinite deposits of the same age in Lower Silesia (Gilg 2003).

The age of *white galman* is assumed to be the same as the sulfide ores. Even though this ore is of minor importance in the Polish mining district, it may represent an uncommon and potentially economic sort of hydrothermal nonsulfide concentration elsewhere. This mineralization is different from both the traditional hypogene ores

classified by Hitzman et al. (2003) and from the newly described Angouran-type mineralization (Boni et al. 2007), related to the waning phases of Tertiary volcanic activity in the Zagros chain (Iran).

Acknowledgements Without the help and guidance of the late Prof. W. Zabinsky of the Mining Academy in Cracow, this study would have probably never been initiated. We are also indebted to M. Szuwarzynski, H. Kucha, A. Paulo, and M. Krzak (Poland) for help and stimulating discussion. We would like to thank also the geologists of the Trzebionka and Pomorzany mines for having guided our team and for extra samples. V. Coppola wishes to thank R. Herrington and the staff of EMMA division at the Natural History Museum, London, for the analytical support during an ACCORD project. Special thanks is due to Bernd Lehmann and to an unknown referee for careful reviews and editing.

References

Alexandrowicz SW (1969) Utwory paleogenu w poludniowej części Wyżyny Krakowskiej (Couches de Paléogène de la partie méridionale du Plateau de Cracovie). Rocznik Polskiego Towarzystwa Geologicznego (Annales Societatis Geologorum Poloniae) 39:681–694

Assmann P (1944) Die Stratigraphie der oberschlesischen Trias. I. Der Muschelkalk. Abhandlungen des Reichsamts für Bodenforschung, N.F. 208:124

Bak B (1993) Ferroan dolomites and ankerites from the Silesian–Krakow deposits of zinc and lead ores. Geol Q 37:279–290

Bak B, Nieć M (1978) The occurrence of monheimite in the Boleslaw Zn–Pb ore deposits near Olkusz. Mineral Pol 9:123–128

Bak B, Zabinski W (1981) On the continuity of the solid solution series smithsonite–siderite. Mineral Pol 12:75–80

Belogub EV, Novoselov KA, Yakovleva VA, Spiro B (2008) Supergene sulphides and related minerals in the supergene profiles of VHMS deposits from the South Urals. Ore Geol Rev 33:239–254

Bodnar RJ, Sterner MS (1987) Synthetic fluid inclusions. In: Ulmer GC, Barnes HL (eds) Hydrothermal experimental techniques. Wiley, New York, pp 423–457

Bogacz K, Dzulynski S, Haranczyk C, Sobczynski P (1975) Origin of the ore-bearing dolomite in the Triassic of the Krakow–Silesian Pb–Zn ore district. Annales de la Société Géologique de Pologne 45:139–155

Boni M, Gilg HA, Aversa G, Balassone G (2003) The "Calamine" of SW Sardinia (Italy): geology, mineralogy and stable isotope geochemistry of a supergene Zn-mineralization. Econ Geol 98:731–748

Boni M, Gilg HA, Balassone G, Schneider J, Allen CA, Moore F (2007) Hypogene Zn carbonate ores in the Angouran deposit, NW Iran. Miner Depos 42(8):799–820

Breithaupt A (1841) Vollständiges Handbuch der Mineralogie 2:252

Cabala J (2001) Development of oxidation in Zn–Pb deposits in Olkusz area. In: Mineral deposits at the beginning of the 21st century. Piestrzynsky A, et al (eds) Proceedings Sixth Biennial SGA Meeting Krakow:121–124

Cerling TE (1984) The stable isotope composition of modern soil carbonate and its relationship to climate. Earth Planet Sci Lett 71:229–240

Chang LLJ, Howie RA, Zussmann J (1995) Rock-forming minerals. Non-Silicates: vol. 5B, Longman, London: 392

Church SE, Vaughn RB, Gent CA, Hopkins RT (1996) Lead-isotopic, sulfur isotopic, and trace-element studies of galena from the Silesia–Krakow Zn–Pb ores, polymetallic veins from Góry Świętokrzyskie Mts. and Mysków porphyry copper deposit, Poland. Pr Inst Geol 154:139–155

Cooper BJ, Gibbs GV, Ross FK (1981) The effects of heating and dehydration on the crystal structure of hemimorphite up to 600° C. Zeitschrift für Kristallographie 156:305–321

Coppola V, Boni M, Gilg HA, Balassone G, Dejonghe L (2008) The "calamine" nonsulfide Zn–Pb deposits of Belgium: petrographical, mineralogical and geochemical characterization. Ore Geol Rev 33:187–210

Czaja M (1978) New data on tarnowskite (tarnowitzite) from Tarnowskie Gory. Mineral Pol 9:89–96

Dubinska E, Sakharov BA, Kapron G, Bylina P, Kozubowski JA (2000) Layer silicates from Szklary (Lower Silesia): from ocean floor metamorphism to continental chemical weathering. Geologica Sudetica 33(2):85–106

Dzulynski S (1953) Tektonika poludniowej czesci Wyzyny Krakowskiej. Acta Geol Pol 3:325–441

Effenberger H, Mereiter K, Zemann J (1981) Crystal structure refinement of magnesite, calcite, rhodochrosite, siderite, smithsonite and dolomite, with discussion of some aspects of the stereochemistry of calcite-type carbonates. Zeitschrift für Kristallographie 156:223–243

Felisiak I (1992) Oligocene–Early Miocene karst deposits and their importance for recognition of the development of tectonics and relief in the Carpathian Foreland, Krakow Region, Southern Poland. Ann Soc Geol Pol 62:173–207

Gilg HA (2003) Ein Beitrag zur Isotopen-Geochemie von Tonmineralien und Tonen. Habilitationschrift. Fakultät Chemie, Technische Universität München

Gilg HA, Struck U, Vennemann T, Boni M (2003) Phosphoric acid fractionation for smithsonite and cerussite between 25 and 72°C. Geochim Cosmochim Acta 67:4049–4055

Gilg HA, Boni M, Hochleitner R, Struck U (2008) Stable isotope geochemistry of carbonate minerals in supergene oxidation zones of Zn–Pb deposits. Ore Geol Rev 33:117–133

Goldstein RH (2001) Fluid inclusions in sedimentary and diagenetic systems. Lithos 55:159–193

Gorecka E (1993) Geological setting of the Silesian–Krakow Zn–Pb deposits. Geol Q 37:127–146

Gorecka E, Kozlowski A, Kibitlewski S (1996) The Silesian–Cracow Zn–Pb deposits, Poland: Considerations on ore-forming processes. In: Gorecka E, Leach DL, Kozlowski A (eds), Carbonate-hosted zinc-lead deposits in the Silesian–Cracow area, Poland, Warsaw, Prace Państwowego Instytutu Geologicznego: 166–181

Götte T, Richter DK (2004) Quantitative high-resolution cathodoluminescence spectroscopy of smithsonite. Mineral Mag 68:199–207

Gruszczyk H, Paulo A (1976) Strefa przejściowa w utworach węglanowych triasu obszaru Olkusza. Kwartalnik Geologiczny 20:737–749

Gruszczyk H, Wielgomas L (1987) Zinc and lead ores in the Silesia–Krakow Triassic. In: Osika R (ed) Geology of poland, Volume VI. Mineral Deposits, Publishing House Wydawnictwa Geologiczne, Warsaw, pp 172–183

Gürich G (1897) Das Mineralreich. In: Hausschatz des Wissens, Abteilung IV (B.6), J. Neumann Verlag, 754 pp

Heijlen W, Muchez Ph, Banks DA, Schneider J, Kucha H, Keppens E (2003) Carbonate-hosted Zn–Pb deposits in Upper Silesia, Poland: origin and evolution of mineralizing fluids and constraints on genetic models. Econ Geol 98:911–932

Hitzman MW, Reynolds NA, Sangster DF, Allen CR, Carman C (2003) Classification, genesis, and exploration guides for nonsulfide zinc deposits. Econ Geol 98:685–714

Kotlicki S, Kubicz A (1974) Trias Slaska Opolskiego. Przewodnik 46 Zjazdu PTG, Opole. Wydawnictwa Geologiczne: 18–26

Kowalski B, Gromada E, Swaldek M (1979) Granulometric and lithopetrographic characteristics of boulder clay from the Witkowska Valley in the Swiety Krzyz Mountains. Rocznik Polskie Towarzystwo Geologiczne 49:343–377

Kozlowski A (1995) Origin of Zn–Pb ores in the Olkusz and Chrzanów districts: a model based on fluid inclusions. Acta Geol Pol 45:83–141

Kucha H (2003) Mississippi Valley Type Zn–Pb deposits of Upper Silesia, Poland. In: Kelly JG, Andrew CJ, Ashton JH, Boland MB, Earls G, Fusciardi L, Stanley G (eds) Europe's major base metal deposits. Irish Association for Economic Geology, Dublin, pp 253–271

Kucha H (2005) Oxysulfides, smithsonite-siderite and Fe-free smithsonite as indicators of conditions of formation of primary and supergene non-sulfide Zn–Pb deposits, Upper Silesia, Poland. ESF Workshop on Nonsulfide Zn–Pb Deposits, 21th–23th April, 2005, Iglesias, Italy, Abstract: 24–25

Kucha H, Czajka K (1984) Sulfide–carbonate relationships in Upper Silesian Zn–Pb deposits (Mississippi Valley type), Poland, and their genesis. Trans Inst Min Metall 93:B12–B19

Lawrence LJ, Rafter TA (1962) Sulfur isotope distribution in sulfides and sulfates from Broken Hill South, New South Wales. Econ Geol 57:217–225

Leach DL, Viets JG 1992. Comparison of the Krakow–Silesian Mississippi Valley-type district, southern Poland, with Mississippi Valley-type districts in North America. USGS, Open-File Report OF/92–704: 72 pp

Leach DL, Viets JG, Kozlowski A, Kibitlewski S (1996) Geology, geochemistry, and genesis of the Silesia–Krakow zinc-lead district, southern Poland. In: Sangster DF (eds) Carbonate-hosted lead-zinc deposits. Society of Economic Geologists, 75th Anniversary Volume, Special Publication 4:144–170

Leach DL, Bradley D, Lewchuk MT, Symons DT, de Marsily G, Brannon J (2001) Mississippi Valley-type lead-zinc deposits through geological time: implications from recent age-dating research. Miner Depos 36:711–740

Libowitzky E, Kohler T, Armbruster T, Rossman GR (1997) Proton disorder in dehydrated hemimorphite; IR spectroscopy and X-ray structure refinement at low and ambient temperatures. Eur J Mineral 9:803–810

Machel HG, Mason RA, Mariano AN, Mucci A (1991) Causes and emission of luminescence in calcite and dolomite. In: Baker CE, Kopp OC (eds) Luminescence microscopy and spectroscopy – qualitative and quantitative applications. Society for Sedimentary Geology, Short Course 25:9–25

McDonald WS, Cruickshank DWJ (1967) Refinement of the structure of the hemimorphite. Zeitschrift für Kristallographie 124:180–191

Migoń P (2007) Geomorphology of granite terrains in Poland. In: Granitoids in Poland, AM Monograph No.1: 355–366

Migoń P, Lidmar-Bergström K (2001) Weathering mantles and their significance for geomorphological evolution of central and northern Europe since the Mesozoic. Earth Sci Rev 56:285–324

Narkiewicz M (1993) Cathodoluminescence study of the ore-bearing and related dolostones in the Triassic of the Silesian–Krakow district. Geol Q 37:265–278

Nieć M, Blajda R, Niedzielski B (1993) Zinc-lead ore deposit in Lower Triassic (Roethian) dolomites at Bolesław (Olkusz region, Poland). Geol Q 37:157–174

Niskiewicz J (2000) The Szklary Massif nickel-bearing weathering cover. Geologica Sudetica 33:107–130

Osman AEM (1989) Smithsonite in the oxidation zone of the Upper Silesia Zn–Pb ore deposits (Orzel Bialy Mine, Bytom Area), Poland. Mineral Pol 20:57–68

Ostrowicki B (1965) Nickel minerals of the weathering zone of serpentinites at Szklary (Lower Silesia). Prace Mineralogiczne, Polska Akademia Naukowe 1:1–92

Palache C, Berman, H Frondel C (1951) The system of mineralogy of James. Dwight Dana and Edward Salisbury Dana. Yale University, vol. II: 539 pp

Panek S, Szuwarzynski M (1974) Rudy utlenione cynku w zlozu kopalni Matylda. Rudy i Metale Niezelazne 19:71–74

Panek S, Szuwarzynski M (1975) Fossil sinkholes with galena mineralization in the vicinity of Chrzanów (Krakow–Silesian region). Rocznik Polskie Towarzystwo Geologiczne 45:177–189

Panek S, Szuwarzynski M (1976) O przedtortonskiej dolinie erozyjnej wypelnionej osadami trzeciorzedowymi w okolicach a (translated title: *A pre-Tortonian valley with Tertiary fill near Chrzanów*). Annales de la Société Géologique de Pologne 46:503–523

Polish Minerals Yearbook (2007) Bilans zasobow kopalin I wod podziemnych w Polsche. Panstwowy Instytut Geologiczny (PIG) ed., Warszawa: 449 pp

Pouchou JL, Pichoir F (1991) Quantitative analysis of homogeneous or stratified micro-volumes applying the model "PAP". In: Heinrich KFJ, Newbury DE (eds) Electron probe quantification. Plenum Press, New York, pp 31–75

Radwanek-Bak B (1982) Zasieg glebokosciowy strefy utlenienia w zlozu rud Zn–Pb Boleslaw. Rudy i Metale Niezelazne 27:220–225

Radwanek-Bak B (1983) Charakterystyka petrograficzna utlenionych rud cynku ze zloz obszaru Boleslawia i Olkusza. Rocznik Polskie Towarzystwo Geologiczne 53:235–254

Radwanski A (1968) Transgresja dolnego tortonu na obszarze wyzyny Miechowskiej i Krakowskiej (translated title: *Lower Tortonian transgression in the Miechow and Kracow uplands)*. Acta Geol Pol 18:387–440

Reichert J, Borg G (2008) Numerical simulation and a geochemical model of supergene carbonate-hosted non-sulphide zinc deposits. Ore Geol Rev 33:134–151

Rosenbaum J, Sheppard SMF (1986) An isotope study of siderites, dolomites and ankerites at high temperature. Geochim Cosmochim Acta 50:1147–1150

Rosenberg PE, Champness PE (1989) Zincian dolomites and associated carbonates from the Warynski Mine, Poland; an AEM investigation. Am Mineral 74:461–465

Różkowski A, Rudzinska T, Bukowy S (1979) Thermal brines as a potential source of the ore mineralization of the Silesia–Cracow Area. Prace Państwowego Instytutu Geologicznego 95:59–85

Sass-Gustkiewicz M (1996) Internal sediments as a key to understanding the hydrothermal karst origin of the Upper Silesian Zn–Pb ore deposits. In: Sangster DF (eds) Carbonate-hosted lead-zinc deposits. Society of Economic Geologists, Special Publication 4:171–181

Sass-Gustkiewicz M, Dzulyński M (1998) Comments on the origin of stratabound Zn–Pb ores in the Upper Silesia, Poland. Ann Soc Geol Pol 68:267–278

Sass-Gustkiewicz M, Dzulyński M, Ridge JD (1982) The emplacement of zinc–lead sulfide ores in the Upper Silesian district—a contribution to the understanding of Mississippi Valley-type deposits. Econ Geol 77:392–412

Sibley DF, Gregg JM (1987) Classification of dolomite rock textures. J Sediment Petrol 57:967–975

Smakowski T, Strzelska-Smakowska B (2005) The calamine ores from the Silesia–Krakow ore province (Poland). ESF Exploratory Workshop Nonsulfide Zn–Pb ores, 21th–23th April, 2005, Iglesias, Italy, Abstract: 35–36

Sobczynski P, Szuwarzynski M, Wojnar E (1978) Formy wystepowania mineralizacji w niecce Chrzanowskiej. Prace Państwowego Instytutu Geologicznego 83:185–192

Swart PK, Burns SJ, Leder JJ (1991) Fractionation of the stable isotopes of oxygen and carbon during reaction of calcite with phosphoric acid as a function of temperature and methods. Chem Geol 86:89–96

Symons DTA, Sangster DF, Leach DL (1995) A Tertiary age from paleomagnetism for Mississipi Valley-type zinc–lead mineralization in Upper Silesia, Poland. Econ Geol 90:782–794

Szuwarzynski M (1978) Eluwialne i supergeniczne kruszce w utworach trzeciorzedowych z okolic Chrzanowa. Rudy i Metale Niezelazne 23:345–349

Szuwarzynski M (1993) The lead and zinc ore deposits in the vicinity of Chrzanów. Geol Q 37(2):209–228

Viets JG, Hofstra AH, Emsbo P (1996) The composition of fluid inclusions in ore and gangue minerals from Mississippi Valley-type Zn–Pb deposits of the Krakow–Silesian region of southern Poland: Genetic and environmental implications; In: Gorecka E, Leach DL, Kozlowski A (eds) Carbonate hosted zinc-lead deposits in the Silesian–Krakow area, Poland. Prace Państwowego Instytutu Geologicznego: 166–181

Wilk Z (1989) Hydrogeological problems of the Krakow–Silesia Zn–Pb ore deposits. In: Bosak P, Ford DC, Glazek J, Horacek I (eds) Paleokarst, a systematic and regional review. Developments in Earth Surface Processes: 513–531

Wyczolkowski J (1974) Stratygrafia piaskowaca pstrego i dolnego wapienia muszlowego polnocno-wschodniego obrzezenia Gornoslaskiego Zaglebia Weglowego w swietle badan paleogeograficznych i sedymentologicznych. Biuletyn Państwowego Instytutu Geologicznego 278:71–114

Yapp CJ (1997) An assessment of isotopic equilibrium in goethites from a bog iron deposit and a lateritic regolith. Chem Geol 135:159–171

Zabinski W (1958) Ferrogalmei (monheimite-galmei) from Katy near Chrzanów. Bulletin of the Academy of Polish Science, Series Science Chemistry, Geology, Geography 6:389–393

Zabinski W (1959) Zincian dolomite from Warynski mine, Upper Silesia. Bulletin of the Academy of Polish Science, Series Science Chemistry, Geology, Geography 7:355–358

Zabinski W (1960) Charakterystyka mineralogiczna strefy utlenienia slasko-krakowskich zloz kruszcow cynku i olowiu. Prace Państwowego Instytutu Geologicznego 1:7–99

Zabinski W (1980) Zincian dolomite: the present state of knowledge. Mineral Pol 2:9–31

Zabinski W (1986) Zincian dolomite: the present state of knowledge. A supplement to Mineral Pol 17:69–71